

Key Points:

- Within the first decades the AMOC weakens under reduced and strengthens under enhanced wind stress forcing
- After a few decades the AMOC drifts toward the reference state under enhanced wind stress while it remains weak under reduced wind stress
- Changes in subpolar North Atlantic and Nordic Seas circulation and climate contribute to the AMOC response

Correspondence to:

K. Lohmann,
katja.lohmann@mpimet.mpg.de

Citation:

Lohmann, K., Putrasahan, D. A., von Storch, J.-S., Gutjahr, O., Jungclaus, J. H., & Haak, H. (2021). Response of northern North Atlantic and Atlantic meridional overturning circulation to reduced and enhanced wind stress forcing. *Journal of Geophysical Research: Oceans*, 126, e2021JC017902. <https://doi.org/10.1029/2021JC017902>

Received 16 AUG 2021

Accepted 20 OCT 2021

Response of Northern North Atlantic and Atlantic Meridional Overturning Circulation to Reduced and Enhanced Wind Stress Forcing

K. Lohmann¹ , D. A. Putrasahan¹ , J.-S. von Storch^{1,2} , O. Gutjahr^{1,3} ,
J. H. Jungclaus¹ , and H. Haak¹ 

¹Max Planck Institute for Meteorology, Hamburg, Germany, ²Center for Earth System Research and Sustainability (CEN), University of Hamburg, Hamburg, Germany, ³Institut für Meereskunde, University of Hamburg, Hamburg, Germany

Abstract Surface wind stress strongly influences Atlantic meridional overturning circulation (AMOC) variability on interannual time scales. On longer time scales, however, its role in AMOC variations is less clear. Here, we show a nonlinear AMOC response to globally reduced and enhanced wind stress forcing, based on sensitivity experiments with MPI-ESM1.2. Under reduced wind stress forcing, the AMOC strength strongly decreases. In contrast, under enhanced wind stress forcing the AMOC strength increases only in the first decades and then decreases, stabilizing at a value similar to the reference simulation. To reveal possible mechanisms underlying this response, we assess the response of the northern North Atlantic circulation and climate to the changed wind stress forcing. Initially, the response is linear: reduced wind stress forcing weakens the gyre circulation and the associated heat and salt transport, leading to larger winter sea ice extent and a shutdown of subpolar deep convection. In the Nordic Seas, the fresher and lighter subsurface state leads to a decrease in the baroclinic pressure and the overflow strength. Under enhanced wind stress forcing, initially, the opposite is happening. However, eventually, subpolar surface density anomalies are determined by warmer temperature rather than increased salinity, leading to a decrease in surface density and a weakening of subpolar deep convection. The resulting AMOC weakening reduces the Atlantic inflow salinity, and subsequently the Nordic Seas baroclinic pressure and overflow strength. The quasi-equilibrium response of the northern North Atlantic circulation and climate under enhanced wind stress forcing differs from the reference simulation, even though the AMOC strength converges.

Plain Language Summary The Atlantic meridional overturning circulation (AMOC) strongly impacts the climate in northwestern Europe through the related northward heat (and salt) transport. Here, we show a nonlinear response of the AMOC to reduced and enhanced wind stress forcing, based on sensitivity experiments with the MPI-M climate model. Under reduced wind stress forcing, the AMOC strength strongly decreases. In contrast, under enhanced wind stress forcing the AMOC strength increases only initially, then decreases and stabilizes at a value similar to the AMOC strength under unchanged wind stress forcing. The initial linear AMOC response to reduced (enhanced) wind stress forcing involves a shutdown (intensification) of both subpolar deep water formation and export of deep water masses from the Nordic Seas. The afterward different response under enhanced wind stress forcing is mainly caused by the fact that eventually subpolar surface density anomalies are determined by temperature (decrease in density due to warming) rather than salinity anomalies (increase in density due to increased salinity), which leads to a decrease in surface density and to a weakening of subpolar deep water formation.

1. Introduction

Surface wind stress determines the variability of the Atlantic meridional overturning circulation (AMOC) both on shorter (intra-to-interannual) time scales by affecting its local Ekman component (Bjastoch et al., 2008; Eden & Willebrand, 2001; Evans et al., 2017; Koehl, 2005; Xu et al., 2014;) and on long time scales by wind-induced Ekman upwelling of dense water masses in the Southern Ocean (Delworth &

© 2021. The Authors.

This is an open access article under the terms of the [Creative Commons Attribution License](https://creativecommons.org/licenses/by/4.0/), which permits use, distribution and reproduction in any medium, provided the original work is properly cited.

Zeng, 2008; Marshall & Speer, 2012; Toggweiler & Samuels, 1995). On decadal time scales, however, the role of the surface wind stress in AMOC variability is unclear (Buckley & Marshall, 2016).

A frequently proposed mechanism, based on model studies, relates decadal AMOC variability to changes in North Atlantic deep convection and/or Nordic Seas overflows (Ba et al., 2013; Bentsen et al., 2004; Danabasoglu et al., 2012; Delworth et al., 1993; Dong & Sutton, 2005; Jungclauss et al., 2005; Koehl & Stammer, 2008; Mauritzen & Haekkinen, 1999; Medhaug et al., 2012; Msadek & Frankignoul, 2009; Zhang et al., 2011). Wind stress contributes to AMOC variability of subpolar or Nordic Seas origin by Ekman upwelling of dense water in the North Atlantic deep water formation sites and by affecting the strength of the North Atlantic gyre circulation and thus the northward advection of warm and salty water from the subtropics (Danabasoglu, 2008; Dong & Sutton, 2005; Frankignoul et al., 2009; Jackson & Vellinga, 2012; Mikolajewicz & Voss, 2000; Putrasahan et al., 2019).

Despite the important role that wind stress plays in AMOC variability, there are few studies that address the AMOC response to changed wind stress forcing over the North Atlantic, and the results are contradictory. In the absence of wind stress forcing over the North Atlantic, the AMOC strength decreases strongly at all latitudes in the North Atlantic (Cessi, 2018). By doubling the wind stress forcing poleward of 30° latitude in both hemispheres in a long (order 1,000 years) ocean model simulation configured in an idealized Atlantic basin, Klinger et al. (2003) find a decrease in the AMOC strength at all latitudes in the North Atlantic. Using a similar model setup and doubling the wind stress forcing over the North Atlantic, Cessi (2018) finds an increase in the maximum AMOC strength in the subpolar North Atlantic, but a decrease in the AMOC strength at other latitudes in the North Atlantic. By globally doubling the wind stress forcing in a 30-year long eddy-resolving ocean model simulation, Lueschow et al. (2021) and Rohrschneider et al. (2021) find a strengthening of the AMOC at all latitudes in the North Atlantic. However, comparison with a simulation in which only the westerlies over the Southern Ocean are doubled suggests that a large part of the AMOC strengthening in the North Atlantic is caused by remote wind stress forcing over the Southern Ocean (Lueschow et al., 2021).

In a recent study, Putrasahan et al. (2019) suggest that the strong decline in the AMOC strength in a version of the Max Planck Institute for Meteorology Earth System Model (MPI-ESM1.2) that applies a higher-resolution atmospheric grid configuration is mainly caused by weaker surface winds compared to the standard-resolution version used in the sixth phase of the Coupled Model Intercomparison Project (CMIP6; Eyring et al., 2016). The weak surface winds spin down the North Atlantic gyre circulation, thereby reducing the northward heat and salt transport. The colder and fresher conditions in the subpolar North Atlantic lead to a large increase in sea ice extent, which prevents deep convection. Apart from subpolar deep water formation, the overflow water masses from the Nordic Seas constitute about two-third of the AMOC strength, including entrained ambient water downstream of the Greenland-Scotland-Ridge (GSR) (Dickson & Brown, 1994). The role of the Nordic Seas overflows in the AMOC decline under reduced wind stress forcing is, however, only marginally discussed in Putrasahan et al. (2019).

Here, we perform sensitivity experiments with the CMIP6 standard-resolution version of MPI-ESM1.2, in which the mean coupling wind stress is either globally reduced (factor of 0.5) or enhanced (factor of 2). This setup allows us to investigate a possible nonlinear response of the ocean to reduced and enhanced wind stress forcing. In contrast to the idealized Atlantic basin applied in Klinger et al. (2003) and Cessi (2018), our global setup also allows us to discuss the role of the Nordic Seas circulation and climate as well as the exchanges across the GSR in the AMOC response to the changed wind stress forcing.

The study is organized as follows: In Section 2, we describe the design of the wind sensitivity experiments as well as the simulated AMOC state. In Sections 3–5, we assess the initial and quasi-equilibrium response of the northern North Atlantic circulation and climate as well as the AMOC to reduced and enhanced wind stress forcing. In Section 6, we assess the Ekman component of the AMOC in the wind sensitivity experiments. Our results are summarized and discussed in Section 7.

2. Wind Sensitivity Experiments

2.1. Experimental Setup

Our study is based on MPI-ESM1.2 (version 1.2.01) (Mauritsen et al., 2019), consisting of the atmosphere component ECHAM6.3 including the land-surface scheme JSBACH, the combined ocean and sea ice component MPIOM1.6.3 and the ocean biogeochemical component HAMOCC. Ocean and atmosphere are coupled by OASIS3 with a coupling frequency of 1 h.

We use the CMIP6 standard-resolution configuration denoted as MPI-ESM1.2-HR. A spectral grid at truncation T127 (about 1°) and 95 hybrid levels are used for the atmosphere component. A tripolar grid (two northern poles) with a nominal resolution of 0.4° (eddy-permitting) and 40 unevenly spaced depth levels are used for the ocean component. A partial grid cell formulation (Adcroft et al., 1997; Wolff et al., 1997) is used to better represent the bottom topography. The performance of the MPI-ESM1.2-HR configuration is evaluated in Mueller et al. (2018) and Gutjahr et al. (2019).

As reference simulation, we take a 250-year long control simulation from the CMIP6 High Resolution Model Intercomparison Project (HighResMIP) (Haarsma et al., 2016). The simulation is initialized from the observation-based EN4 temperature and salinity data set (Good et al., 2013), taking the mean (seasonal) state of years 1950–1954. It applies the external forcing corresponding to year 1950. Its mean climate is evaluated in Gutjahr et al. (2019) and Gutjahr et al. (2021) (denoted as HR_{pp} in their studies).

In addition, we perform two 250-year long wind sensitivity experiments with the same setup as our reference simulation, in which we either reduce the mean wind stress received by the ocean component by a factor of 0.5 or enhance it by a factor of 2. We choose a factor of 0.5 because this corresponds to the wind stress reduction over the key region of the subpolar North Atlantic in the MPI-ESM1.2 version that applies a higher-resolution atmospheric grid configuration (Putrasahan et al., 2019).

A momentum flux correction, $\Delta\tau$, is applied at every coupling time step as follows:

$$\tau = \bar{\tau} + \Delta\tau + \tau',$$

where τ denotes the wind stress received by the ocean component, the overbar the time mean and τ' the deviation from it. The flux correction is applied to all ocean grid cells which are (partly) ice-free at a particular time step (weighted with the open-water part of the respective grid cell). We note that our flux correction does not take into account wind stress acting on sea ice. The latter, however, only indirectly affects the momentum transfer into the ocean through the coupling of ocean and sea ice velocity.

The flux correction term is given by

$$\Delta\tau = -0.5\bar{\tau}_{control}$$

for the experiment with reduced wind stress forcing, in the following denoted as the “0.5windstress” experiment, and

$$\Delta\tau = \bar{\tau}_{control}$$

for the experiment with enhanced wind stress forcing, in the following denoted as the “2windstress” experiment. Thus, the wind stress received by the ocean component is approximately

$$\tau = 0.5\bar{\tau}_{control} + \tau'$$

in the “0.5windstress” experiment, and

$$\tau = 2\bar{\tau}_{control} + \tau'$$

in the “2windstress” experiment.

$\bar{\tau}_{control}$ is the mean wind stress of the first 20 integration years in the reference simulation. The first 20 integration years are chosen following the design of the sensitivity experiments in Putrasahan et al. (2019). We note that the mean wind stress in the reference simulation does not change significantly over time.

Therefore, the choice of the averaging period should not affect our results. We underline that the amplitude of the wind stress variability (τ') in the wind sensitivity experiments is not modified. We further underline that the applied flux correction affects only the momentum flux, while the buoyancy fluxes (which also depend on the surface wind) remain unchanged, except for the effects of a potential correlation between momentum and buoyancy flux anomalies, for example, changes in sea surface temperature (SST) induced by wind-driven circulation changes.

2.2. AMOC State

In the last 150 integration years (when the AMOC reaches a quasi-equilibrium response), the AMOC is substantially weaker and shallower in the “0.5windstress” experiment compared to the reference simulation (Figures 1a, 1b, and 1d). The decrease in the maximum AMOC strength at 26.5°N is about 50% (6 Sv) (Figure 2a), and the boundary between the North Atlantic Deep Water (NADW) and the Antarctic Bottom Water (AABW) cell is shifted upward by about 500 m (Figures 1a and 1b). The joint variations of strength and depth of the NADW cell are in line with Marshall et al. (2017).

In contrast, the quasi-equilibrium AMOC strength and vertical extent are less affected in the “2windstress” experiment (Figures 1a, 1c, 1e, and 2a). The AMOC in the Nordic Seas (65°–80°N in Figure 1) responds most sensitively to enhanced wind stress forcing, with an AMOC strength that is about 50% (2 Sv) higher than the strength in the reference simulation. In density space (not shown), the AMOC strength also slightly increases in the subpolar North Atlantic (by about 10% or 2 Sv). Such an increase is not found in depth space (Figure 1e), probably due to the strongly inclined isopycnals in the subpolar region.

In contrast to the NADW cell, the AABW cell tends to strengthen under reduced and weaken under enhanced wind stress forcing (Figure 1), in agreement with the concept of the “ocean seesaw” (Broecker, 1998). The wind-driven subtropical cells, as expected, weaken under reduced and strengthen under enhanced wind stress forcing.

Considering the time evolution, the AMOC strength in the “2windstress” experiment indeed shows an increase in the first 20 integration years, and thus initially an opposite behavior to the AMOC strength in the “0.5windstress” experiment (Figure 2a). Afterward, however, the AMOC strength in the “2windstress” experiment decreases, reaching a quasi-equilibrium strength that is approximately equal to the strength in the reference simulation. Thus, three questions are discussed in our study:

1. Do the northern North Atlantic circulation and climate as well as the AMOC initially (within a few decades) respond linearly to reduced and enhanced wind stress forcing?
2. Why is the AMOC strength decreasing (after the initial increase) under enhanced wind stress forcing?
3. What is the quasi-equilibrium response of the northern North Atlantic circulation and climate as well as the AMOC under reduced and enhanced wind stress forcing? To what extent differs the quasi-equilibrium response of the northern North Atlantic circulation and climate under enhanced wind stress forcing from the reference simulation, even though the AMOC strength converges?

3. Initial Response of Subpolar North Atlantic and Nordic Seas Circulation and Climate to Reduced and Enhanced Wind Stress Forcing

Following Putrasahan et al. (2019), we consider the difference between the respective sensitivity experiment and the reference simulation, averaged over the second decade. One-dimensional variables, such as transports, are shown for the entire integration length, but only the evolution in the first decades is discussed in this section. For easier understanding, only the case of enhanced wind stress forcing is described here. In the case of reduced wind stress forcing, the opposite is happening (both cases are shown in the figures). The transient response to reduced wind stress forcing is also investigated in Putrasahan et al. (2019), based on a higher-resolution version of the model, which exhibits weaker surface winds.

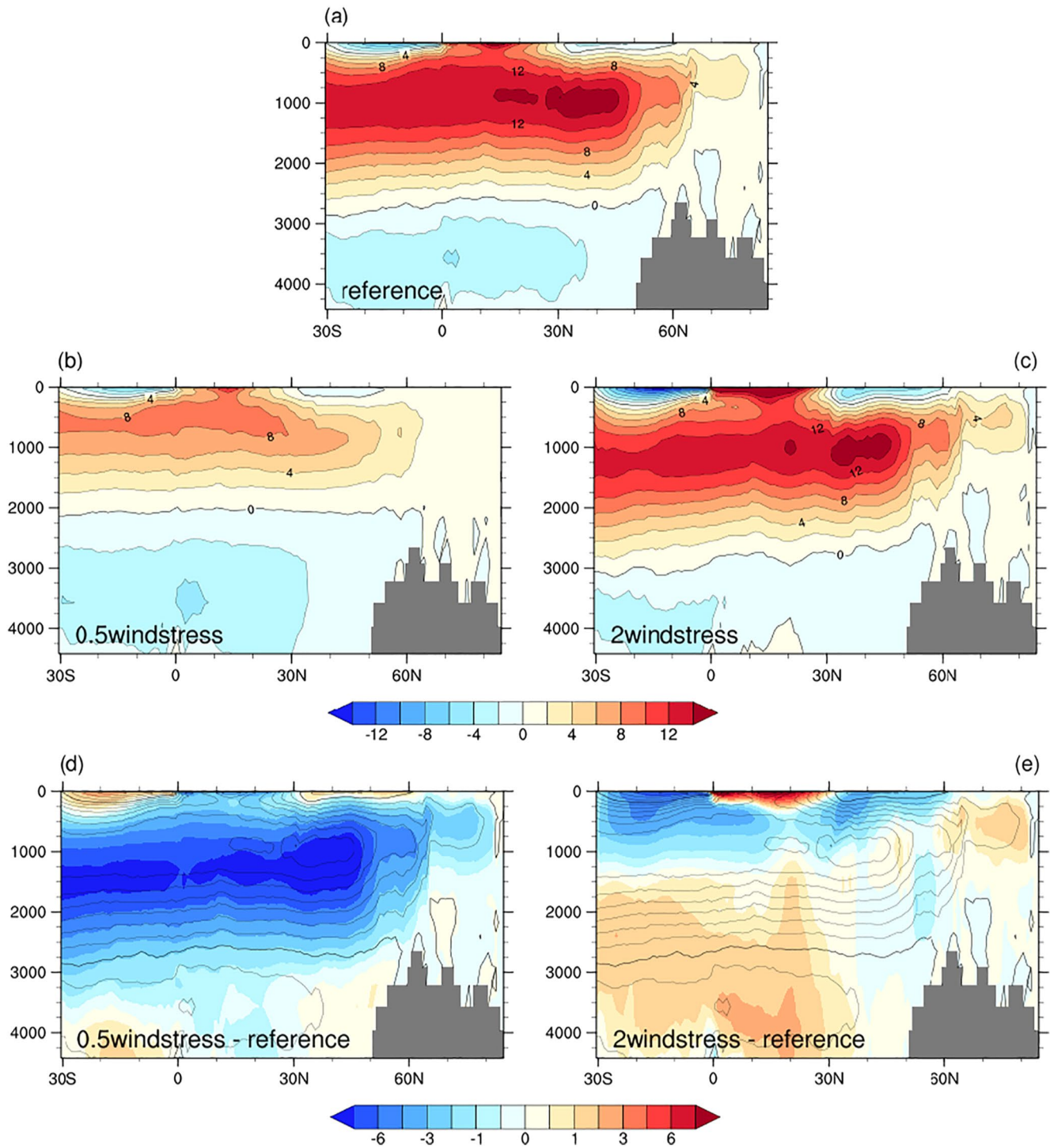


Figure 1. Time mean Atlantic meridional streamfunction [in Sverdrup, $1 \text{ Sv} = 10^6 \text{ m}^3/\text{s}$] averaged over integration years 101–250 in (a) the reference simulation, (b) the “0.5windstress” experiment, and (c) the “2windstress” experiment. Difference of the time mean Atlantic meridional streamfunction averaged over integration years 101–250 between (e) the “0.5windstress” experiment and the reference simulation and (f) the “2windstress” experiment and the reference simulation. Contour lines in the difference plots indicate the time mean Atlantic meridional streamfunction averaged over integration years 101–250 in the reference simulation. We note that contour levels in the difference plots are nonlinear with values [0.5, 1, 2, 3, 4.5, 6, 7.5].

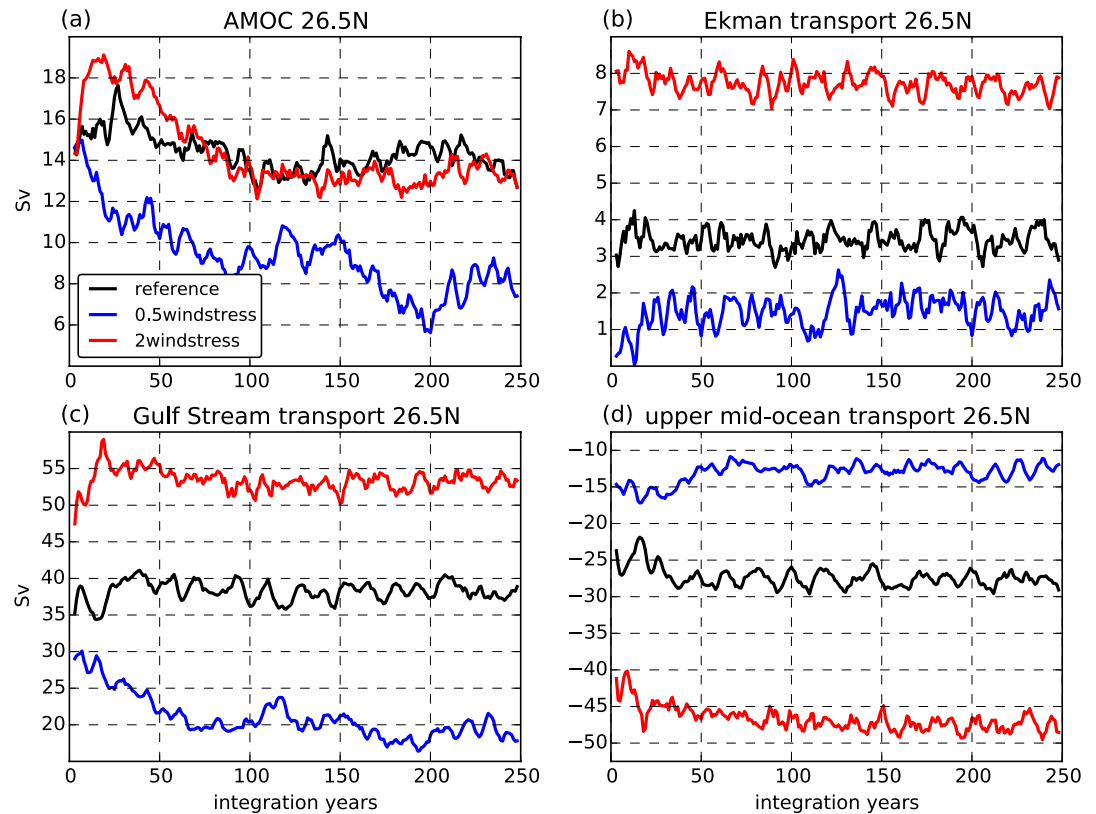


Figure 2. Time series [in Sv] of (a) the AMOC strength at 26.5°N, (b) the Ekman component of the AMOC, (c) the Gulf Stream transport, and (d) the upper mid-ocean transport in the reference simulation (black line), the “0.5windstress” experiment (blue line) and the “2windstress” experiment (red line). For the definition of the Ekman component and the transports see text. Values are annual values with a 5-year running mean applied.

3.1. Initial Response of Subpolar North Atlantic Circulation and Climate

Stronger surface wind stress spins up the North Atlantic gyre circulation (Figures 3b and 4). Stronger gyre circulation leads to enhanced heat and salt transport into the subpolar North Atlantic (Figures 5a and 5c), and subsequently to a warmer and saltier subpolar surface state (Figures 3d and 3h). The strongest warming is found in the western part in areas that are ice-free in winter compared to the reference simulation (Figure 3l). The strong SST anomalies are dampened by the surface heat flux anomalies (tending to decrease SST) (Figure 3f).

The sea surface salinity (SSS) anomalies resemble those in SST. However, reduced surface fresh water input contributes to the saltier SSS in the (western) subpolar region (Figure 3j). The fresh water flux anomalies are caused by enhanced evaporation (Figure 6) due to stronger surface winds and a warmer and less ice-covered surface state. The saltier SSS along the northern rim of the subpolar region is also supported by reduced sea ice export from the Nordic Seas through the Denmark Strait (Figure 7c).

The warmer and saltier surface state leads to a smaller winter sea ice extent in the western subpolar region (Figure 3l), favoring the conditions for deep convection due to increased winter heat loss to the atmosphere. Deep convection is also supported by increased surface density in the western subpolar region (Figure 8b), as initially surface density anomalies are determined by salinity anomalies (Figure 8d; note that the temperature effect on density is multiplied with “−1” for easier comparison). Consequently, subpolar deep convection intensifies, both with respect to convection depth and area covered by convective activity (Figures 3n, 9a, and 9b).

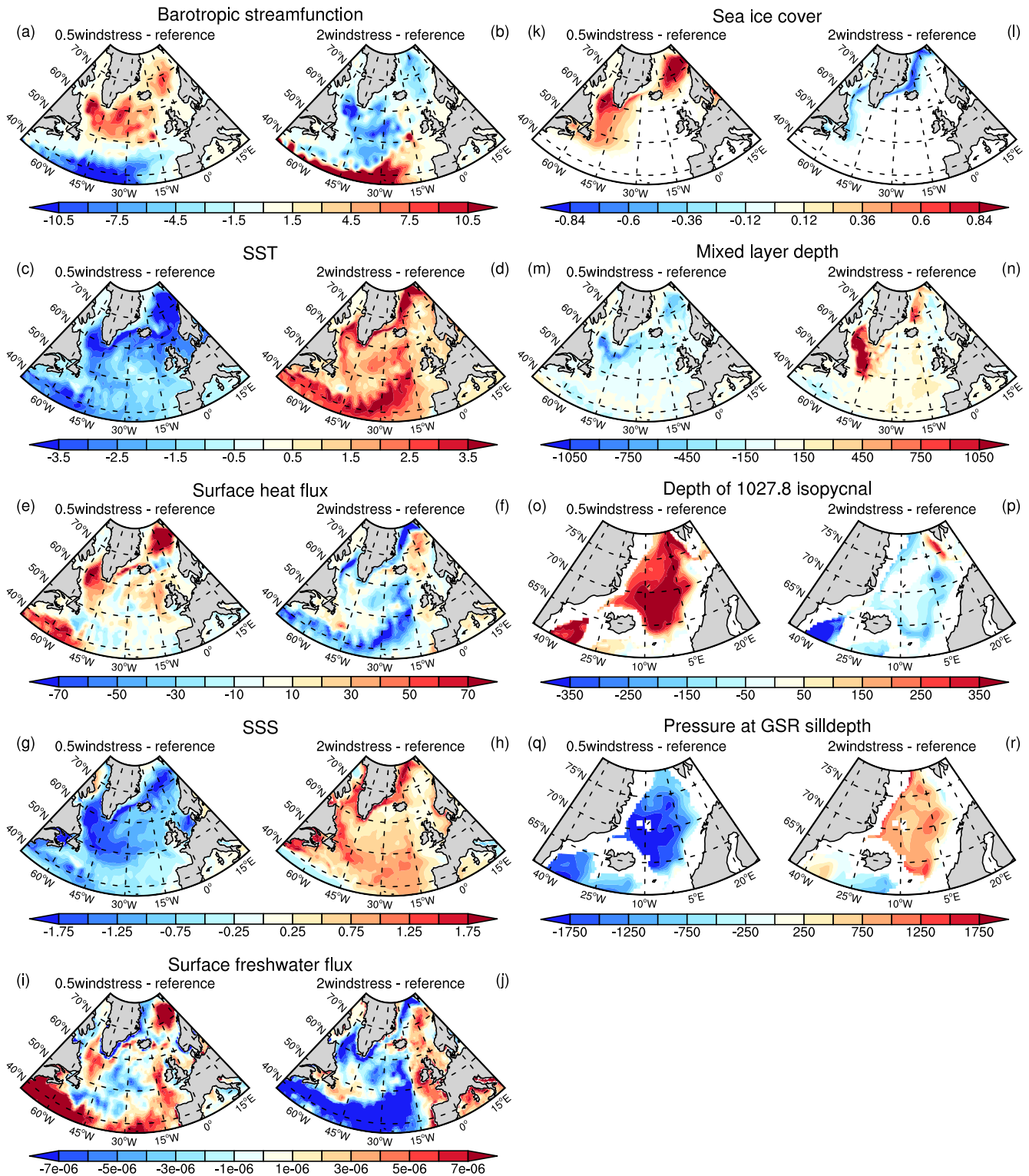


Figure 3. Difference between (left panels) the “0.5windstress” experiment and the reference simulation and (right panels) the “2windstress” experiment and the reference simulation, averaged over integration years 11–20. (a, b) Barotropic streamfunction [in Sv], (c, d) SST [in °C], (e, f) downward surface heat flux [in W/m²], (g, h) SSS [in psu], (i, j) downward surface fresh water flux [in kg/m²s], (k, l) sea ice extent in March [0 to 1, not plotted where sea ice extent is zero in both the respective sensitivity experiment and the reference simulation], (m, n) mixed layer depth in March [in m], (o, p) depth of isopycnal $\sigma_0 = 27.8 \text{ kg/m}^3$ [in m] (upper boundary of overflow water masses), and (q, r) baroclinic pressure at 800 m depth [in Pa; defined as hydrostatic pressure integrated over the water column, not taking into account the sea surface height].

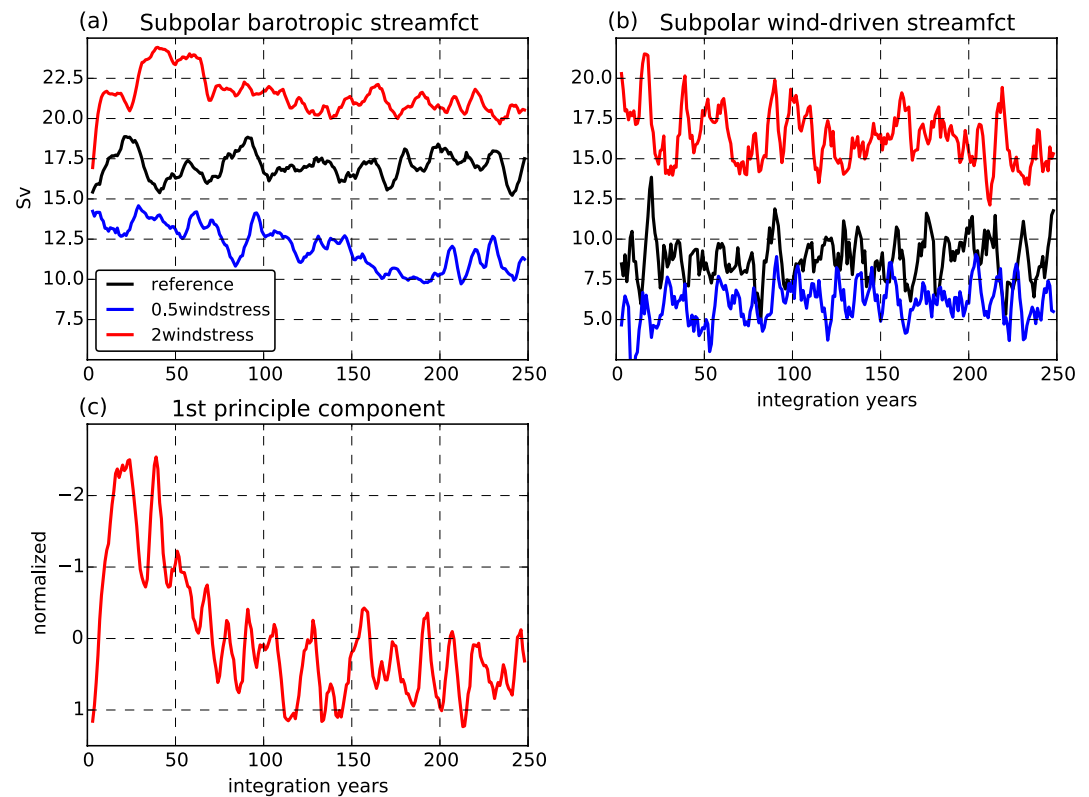


Figure 4. Time series [in Sv, multiplied with “−1”] of (a) the barotropic streamfunction and (b) the wind-driven streamfunction calculated from the Sverdrup relation, averaged over the subpolar North Atlantic (62.5°–15°W, 50°–65°N) in the reference simulation (black line), the “0.5windstress” experiment (blue line) and the “2windstress” experiment (red line). (c) First principle component [normalized, y-axis reversed] of the barotropic streamfunction anomalies in the North Atlantic (80°–5°W, 30°–65°N). Positive (negative) values correspond to a (southward) shift of the boundary between the subtropical and the subpolar gyre in the Newfoundland basin. In all subplots, values are annual values with a 5-year running mean applied.

3.2. Initial Response of Nordic Seas Circulation and Climate

Enhanced northward heat and salt transport under enhanced wind stress forcing is also found across the GSR (Figures 5b and 5d) in line with Biastoch et al. (2003), largely due to an increase in the volume transport of the Atlantic inflow (Figure 7a). Subsequently, a warmer and saltier Nordic Seas surface state develops (Figures 3d and 3h). As in the subpolar North Atlantic, the SST anomalies are dampened by the surface heat flux anomalies (tending to decrease SST) (Figure 3f), whereas reduced surface fresh water input (Figure 3j) contributes to the saltier SSS. An exception is the saltier SSS in the eastern Nordic Seas, which is dampened by enhanced surface fresh water input. We note that this exception does not apply to the case of reduced wind stress forcing, for which enhanced surface fresh water input contributes to the fresher SSS everywhere (Figures 3g and 3i).

Similar to the subpolar North Atlantic, surface density anomalies in the Nordic Seas are determined by salinity anomalies, leading to a denser surface state under enhanced wind stress forcing (not shown). The saltier and denser state is also found regarding salinity and density averaged up to the sill depth of the GSR (Figure 10b for salinity in the “2windstress” experiment), leading to a shallowing of the Nordic Seas isopycnals (Figure 3p) and thus to an increase in the baroclinic pressure at the sill depth of the GSR and the pressure gradient across the ridge (Figure 3r). The latter can explain the strengthening of the overflow branches across the GSR (Figures 11a and 11b) (Hansen & Osterhus, 2007; Jungclauss et al., 2008). We note that in this study overflows are defined as outflow from the Nordic Seas below a depth of 400 m in Denmark Strait and 700 m in Faroe-Shetland Channel. This definition is slightly different from the classical definition of the overflows by density threshold, as it is difficult to apply here, due to the strong decline in the deep densities

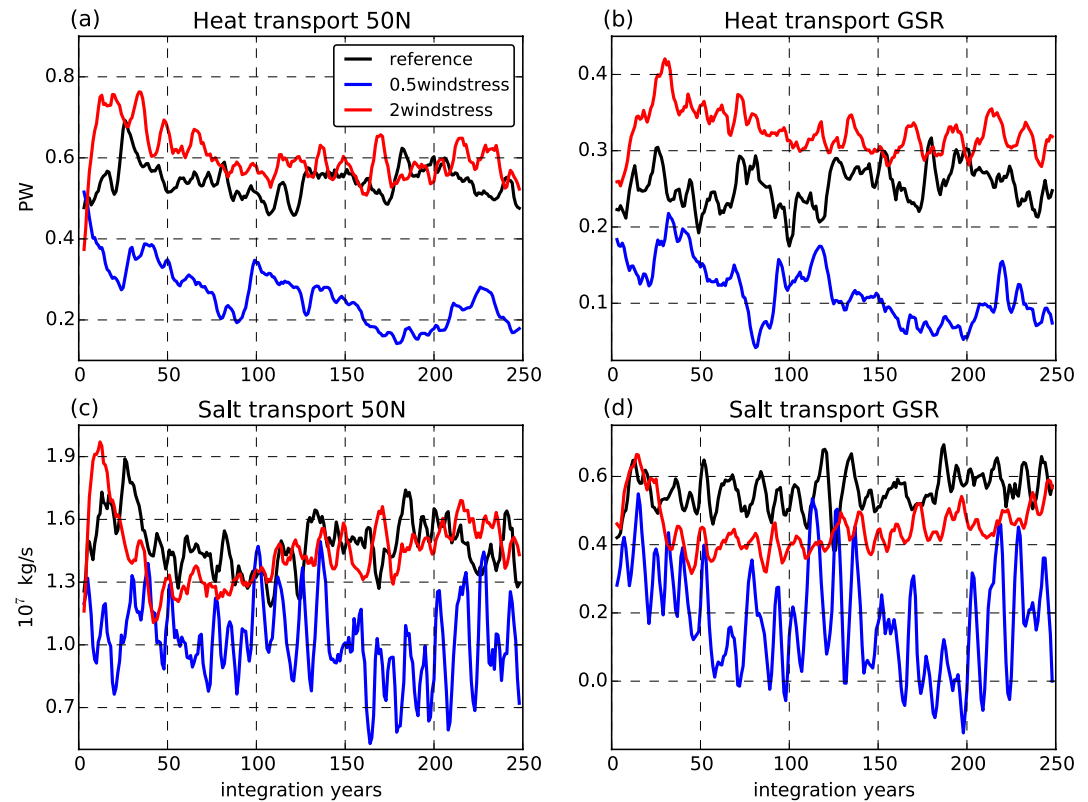


Figure 5. Time series of the heat transport [in PW, reference 0 °C] across (a) 50°N and (b) the GSR, and the salt transport [in 10^7 kg/s, reference 35 psu] across (c) 50°N and (d) the GSR in the reference simulation (black line), the “0.5windstress” experiment (blue line) and the “2windstress” experiment (red line). Values are annual values with a 5-year running mean applied.

along the GSR in the “0.5windstress” experiment (Figures 11c and 11d). The latter results from the warming (2–3°C) of the overflow water masses in this experiment (not shown), probably caused by the shutdown of Nordic Seas deep convection (Figure 3m) due to a large winter sea ice extent (Figure 3k).

In this model setup, changes in the AMOC strength correlate well with variations in both deep convection in the Labrador Sea and Denmark Strait overflow. Thus, the decrease in the “0.5windstress” experiment and

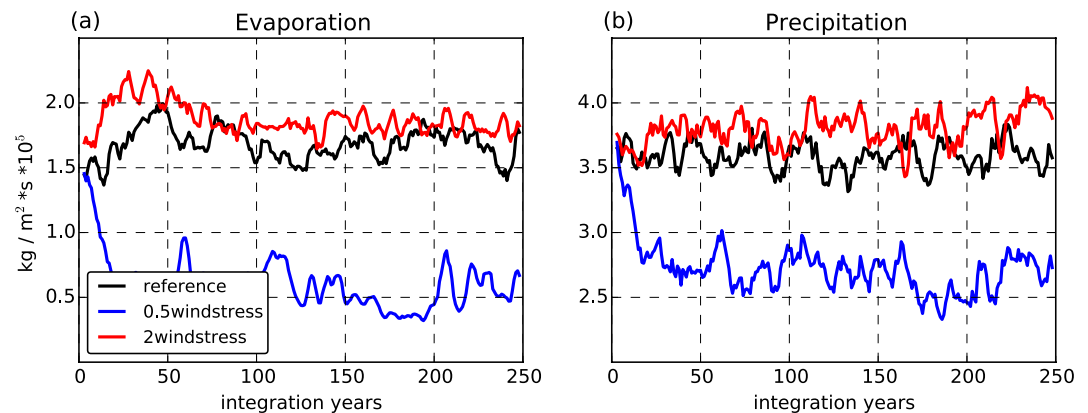


Figure 6. Time series [in 10^{-5} kg/m²s] of (a) the evaporation and (b) the precipitation, averaged over the western subtropical North Atlantic (62.5°–40°W, 50°–65°N) in the reference simulation (black line), the “0.5windstress” experiment (blue line) and the “2windstress” experiment (red line). Values are annual values with a 5-year running mean applied.

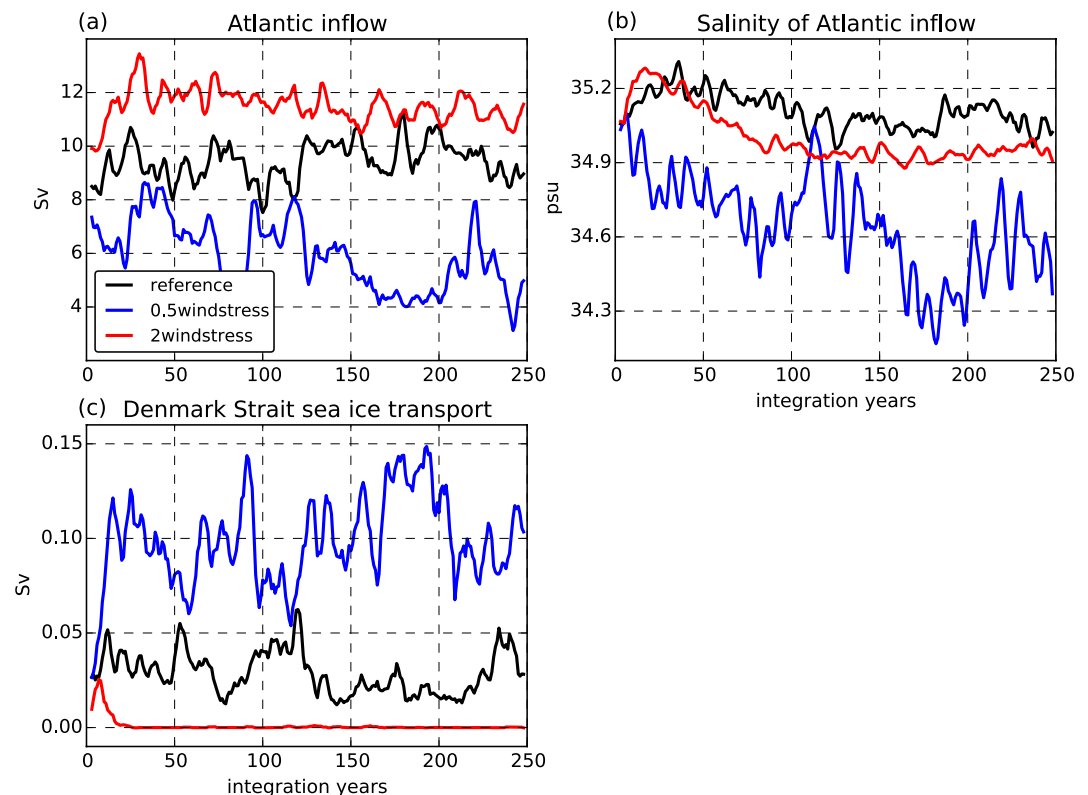


Figure 7. Time series of (a) the volume transport [in Sv] and (b) the salinity [in psu] of the Atlantic inflow across the GSR, and (c) the sea ice volume transport [in Sv, multiplied with “−1”] through the Denmark Strait in the reference simulation (black line), the “0.5windstress” experiment (blue line) and the “2windstress” experiment (red line). The inflow is defined as the sum of the flow into the Nordic Seas through the Denmark Strait and the net flow above 500 m across the Iceland-Scotland-Ridge (to take into account the recirculation). Values are annual values with a 5-year running mean applied.

the intensification in the “2windstress” experiment in both subpolar deep convection and Denmark Strait overflow strength can explain the initially (within a few decades) linear response of the AMOC to reduced and enhanced wind stress forcing (Figure 2a).

4. Why Is the AMOC Strength Declining (After Initially Increasing) Under Enhanced Wind Stress Forcing?

4.1. Contribution of Subpolar North Atlantic Circulation and Climate

Similar to the evolution of the AMOC strength in the “2windstress” experiment (Figure 2a), deep convection in the subpolar North Atlantic intensifies for about 40 years, with decadal variability superimposed (Figure 9a). In the previous section, we link the initial intensification of subpolar deep convection in the “2windstress” experiment to a decrease in winter sea ice extent (Figure 3l) and thus increased exposure to heat loss to the atmosphere, as well as an increase in surface density, because density anomalies are initially determined by salinity anomalies (Figure 8d; note that the temperature effect on density is multiplied with “−1” for easier comparison). The superimposed decadal variability is driven by the atmospheric state, specifically the North Atlantic oscillation (NAO), as a positive NAO is associated with strong winter heat loss to the atmosphere in the western subpolar North Atlantic (Figures 9a and 9c).

After about 40 years, subpolar deep convection remains weaker than initially, despite the occurrence of periods with strongly positive NAO and a generally small winter sea ice extent (Figure 12l for the last 150 integration years). However, after a few decades, a strong decrease (after the initial increase) in western subpolar surface density is found (Figure 8b) that possibly prevents the surface layers from becoming dense

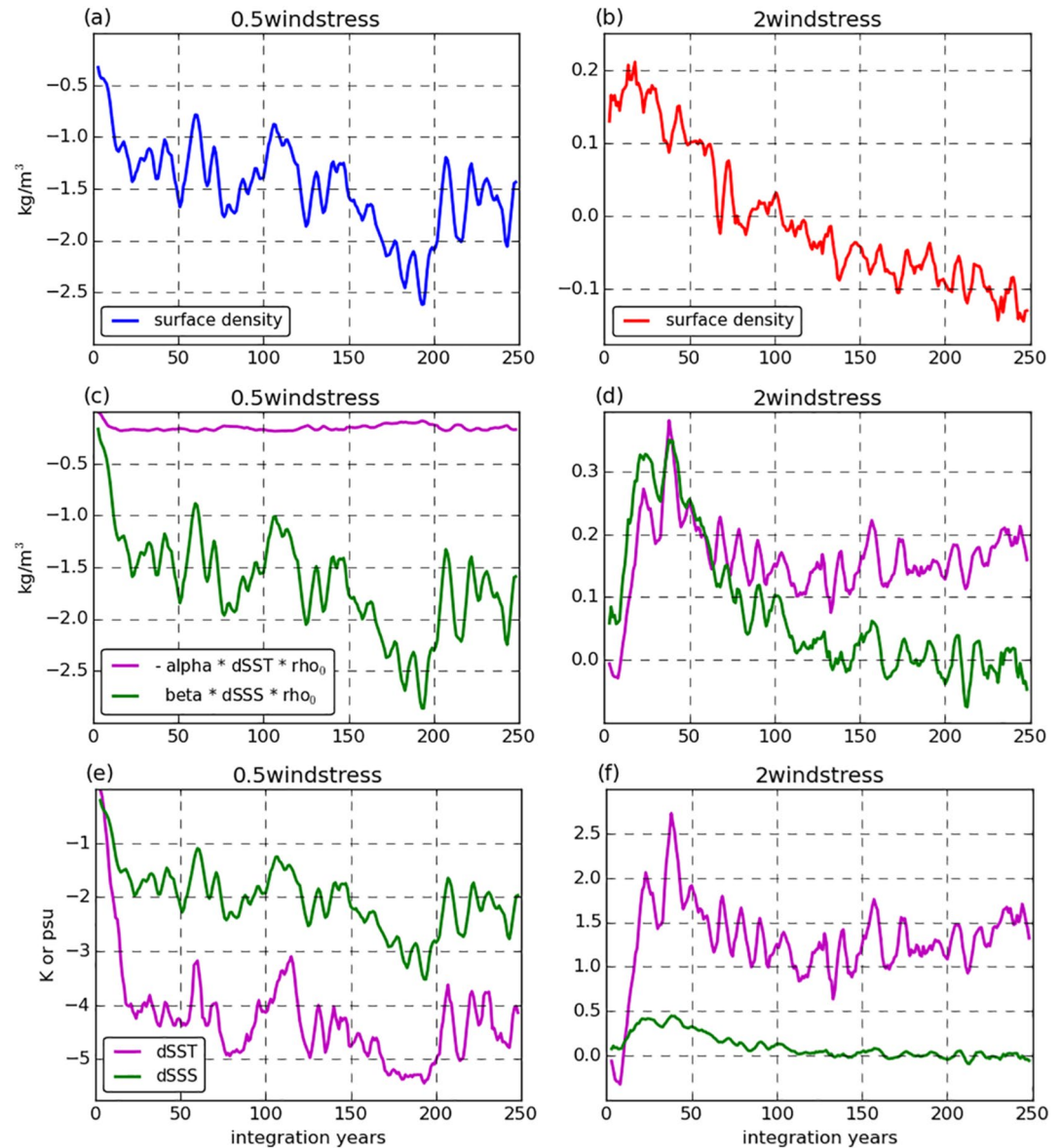


Figure 8. Time series of (a, b) the surface density anomalies [in kg/m^3 , with respect to the first integration year] calculated based on the full equation of state, (c, d) the density anomalies [in kg/m^3 , with respect to the first integration year] related to SST anomalies (magenta line, multiplied with “-1”) and SSS anomalies (green line) calculated based on the linearized equation of state, and (e, f) SST anomalies [in K, with respect to the first integration year] (magenta line) and SSS anomalies [in psu, with respect to the first integration year] (green line), all averaged over the western subpolar North Atlantic ($62.5^\circ\text{--}40^\circ\text{W}$, $50^\circ\text{--}65^\circ\text{N}$) in (left panels) the “0.5windstress” experiment and (right panels) the “2windstress” experiment. A 5-year running mean is applied to the actual SST and SSS values before calculating thermal and haline expansion coefficients. Surface density, SST and SSS anomalies are annual values with a 5-year running mean applied.

enough to be mixed down. The warmer and saltier anomalies in the western subpolar North Atlantic compared to the reference simulation have a compensating effect on density. The decrease in surface density results largely from the fact that, after about 50 years, surface density anomalies are determined by temperature rather than salinity anomalies (Figure 8d).

Splitting the surface density anomalies (based on the linearized equation of state) into thermal and haline expansion coefficients (not shown) as well as SST and SSS anomalies (Figure 8f), suggests that the strong decrease in surface density is primarily caused by the fact that the decrease (compared to the initial increase)

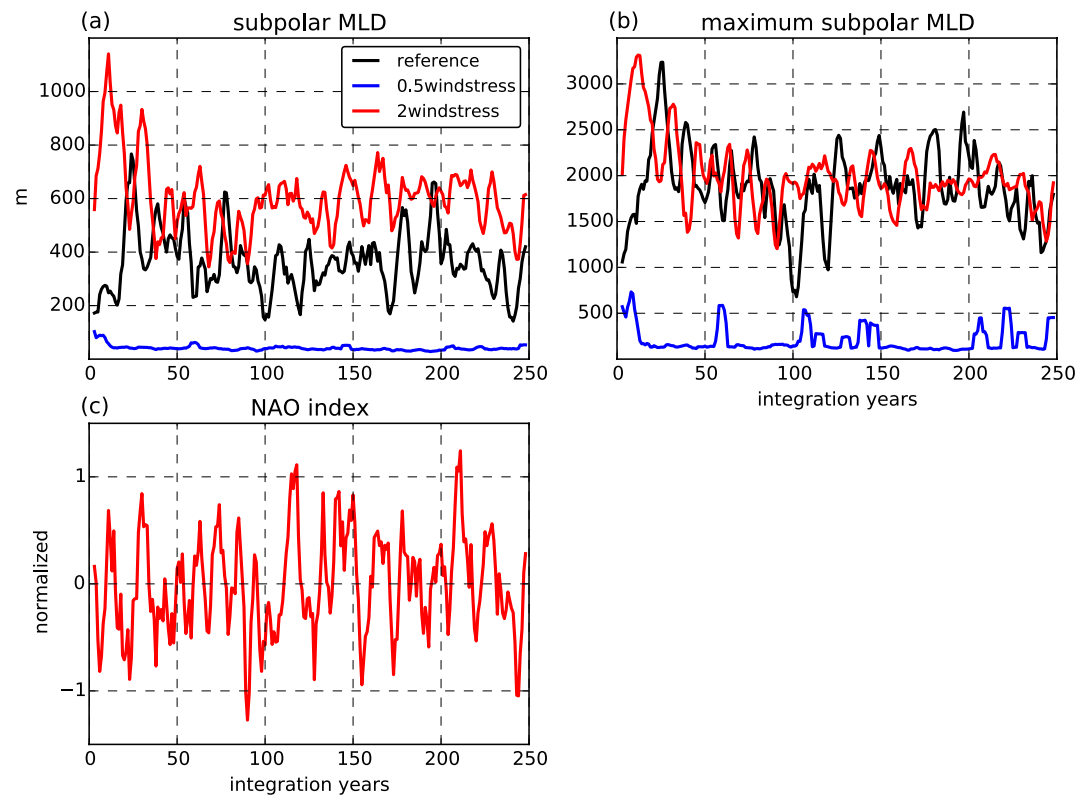


Figure 9. Time series of (a) the mixed layer depth [in m] averaged over the western subpolar North Atlantic (62.5° – 40° W, 50° – 65° N) and (b) the maximum mixed layer depth [in m] in the western subpolar North Atlantic in the reference simulation (black line), the “0.5windstress” experiment (blue line) and the “2windstress” experiment (red line). Values are March values with a 5-year running mean applied. (c) North Atlantic Oscillation index [normalized, with a 5-year running mean applied], defined as the first principle component of the mean sea level pressure (DJFM mean) in the region 70° W– 20° E and 20° – 80° N, in the “2windstress” experiment.

in western subpolar SSS is larger than the decrease in western subpolar SST. One possible explanation for the latter is the increase in surface fresh water input in the western subpolar North Atlantic due to a decrease in evaporation and an increase in precipitation (Figure 6). The surface heat flux in the western subpolar North Atlantic (not shown), in contrast, has a damping effect on the decline in SST.

Apart from the surface fresh water input, the decrease in western subpolar SST and SSS results from a weaker heat and salt transport across 50° N (Figures 5a and 9c), largely of the gyre component (not shown). The weakening of the salt transport starts earlier and is larger than the weakening of the heat transport, which provides another possible explanation why the decrease in SSS is larger than the decrease in SST.

The reason for the changes in the gyre component of the heat and salt transport across 50° N is not clear. Partly the changes resemble the first principle component of the barotropic streamfunction anomalies in the North Atlantic (Figure 4c). The corresponding empirical orthogonal function (not shown) largely represents the meridional shift of the boundary between the subtropical and subpolar gyre in the Newfoundland basin. After a few decades, the initial southward shift of the gyre boundary is replaced by a northward shift. The shift is also visible in the initial and quasi-equilibrium response of the barotropic streamfunction to enhanced wind stress forcing (Figures 13a and 13b).

The response of the wind-driven streamfunction and the density-driven streamfunction suggests that the northward shift of the gyre boundary is caused by an eventually weaker density-driven component in the western subpolar gyre. The changes in the density-driven gyre component may be related to the changes in subpolar deep convection (Figure 9a). In this case, changes in subpolar deep convection would feedback on the western subpolar surface density by modulating the heat and salt transport across 50° N (via the shift in the gyre boundary).

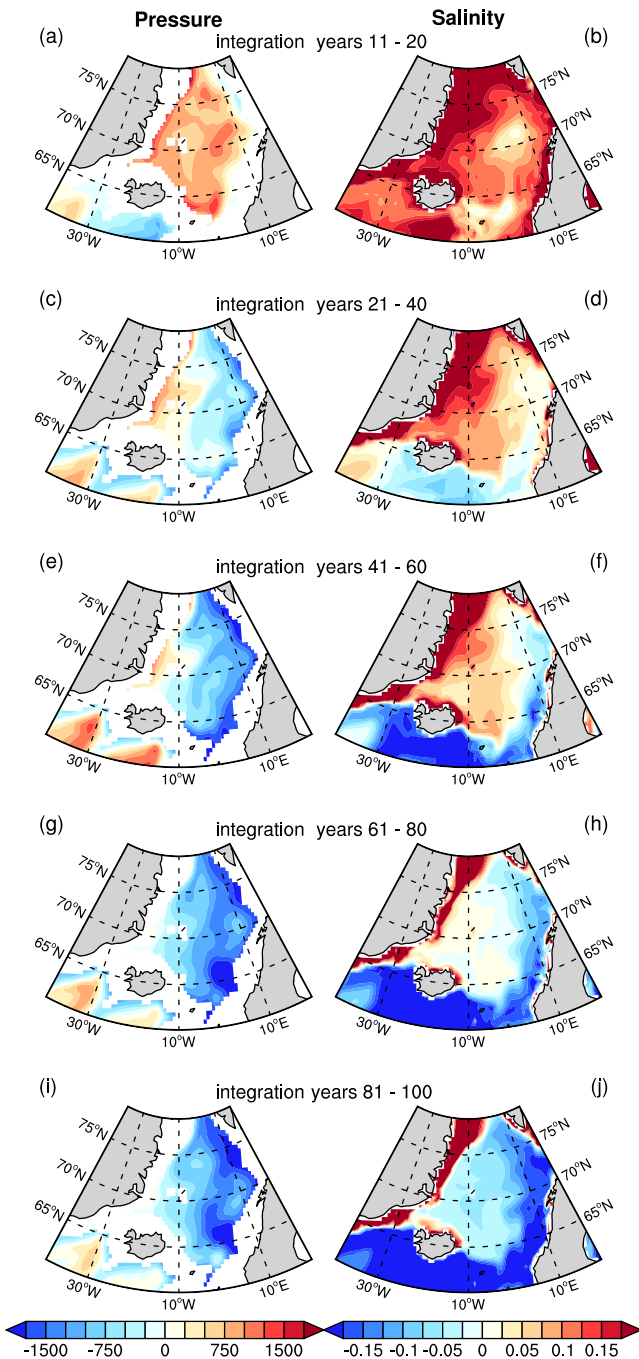


Figure 10. Difference between the “2windstress” experiment and the reference simulation for (left panels) the baroclinic pressure at 800 m depth [in Pa; defined as hydrostatic pressure integrated over the water column, not taking into account the sea surface height] and (right panels) the salinity averaged between the surface and 800 m depth [in psu], averaged over integration years (a, b) 11–20, (c, d) 21–40, (e, f) 41–60, (g, h) 61–80, and (i, j) 81–100. We note that (a) is identical to Figure 3p, but is repeated here to show the time evolution.

4.2. Contribution of Nordic Seas Circulation and Climate

Apart from deep convection in the Labrador Sea, the strength of the overflow through the Denmark Strait correlates well with changes in the AMOC strength in this model setup, while the influence of the overflow through the Faroe-Shetland Channel on AMOC strength is less clear. The weakening of the Denmark Strait overflow in the “2windstress” experiment (from about integration year 75 onwards, Figure 11a) lags behind the AMOC weakening (from about integration year 50 onwards, Figure 2a). Thus, changes in the Nordic Seas overflows are probably not the primary cause for the AMOC weakening in the “2windstress” experiment, but they contribute to maintain the weaker AMOC state afterward. Therefore, we discuss possible mechanisms for a weakening of the Nordic Seas overflows (after an initial strengthening) under enhanced wind stress forcing.

As we suggest in the previous section, the initial strengthening of the overflows can be explained by an increase in the Nordic Seas baroclinic pressure at the sill depth of the GSR (Figure 3r) due to the saltier and denser (sub)surface state compared to the reference simulation. Over time, the saltier subsurface state is gradually replaced by fresher water masses (right panels in Figure 10). With a simultaneous, persistently warmer state (not shown), this freshening reduces the Nordic Seas baroclinic pressure at the sill depth of the GSR (left panels in Figure 10), and thus the overflow transports (Figures 11a and 11b). The gradual decrease in baroclinic pressure starts in the eastern part of the Nordic Seas, which might explain why the Faroe-Shetland Channel overflow weakens earlier than the Denmark Strait overflow.

The gradual freshening of the Nordic Seas over time seems to originate in the subpolar North Atlantic and spread along the flow path of the Atlantic inflow (right panels in Figure 10). Consistently, the salinity of the Atlantic inflow and the salt transport across the GSR in the “2windstress” experiment start to decrease after a few decades, and remain smaller than the respective value in the reference simulation (Figures 5d and 7b). The inflowing salinity is strongly determined by the AMOC strength (comparison of Figures 2a and 7b). Therefore, a weaker AMOC due to declining subpolar deep convection decreases the overflow transports.

5. Quasi-Equilibrium Response of Subpolar North Atlantic and Nordic Seas Circulation and Climate Under Reduced and Enhanced Wind Stress Forcing

After the initially linear response, the AMOC strength (Figures 1 and 2a) and probably also the northern North Atlantic circulation and climate in general, respond nonlinearly to reduced and enhanced wind stress forcing, until the AMOC stabilizes in the last 150 integration years. The latter we refer to as quasi-equilibrium response.

5.1. Quasi-Equilibrium Response to Reduced Wind Stress Forcing

Under reduced wind stress forcing, the quasi-equilibrium response of the subpolar North Atlantic and Nordic Seas circulation and climate is similar to the initial response discussed in Section 3, but the difference to the reference simulation is even larger.

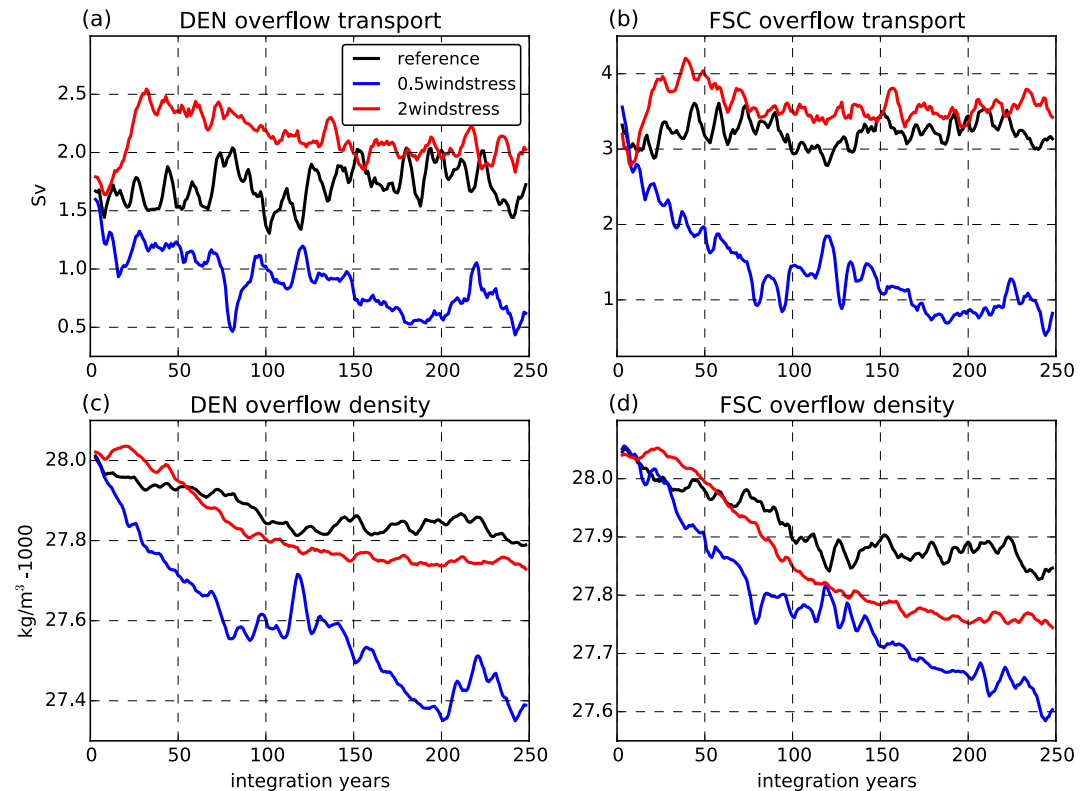


Figure 11. Time series of the overflow volume transport [in Sv, multiplied with “−1”] through (a) Denmark Strait and (b) Faroe-Shetland Channel, and the density [in kg/m³] of the overflow through (c) Denmark Strait and (d) Faroe-Shetland Channel in the reference simulation (black line), the “0.5windstress” experiment (blue line) and the “2windstress” experiment (red line). For the definition of the overflows from the Nordic Seas see text. Values are annual values with a 5-year running mean applied.

The subpolar gyre weakens by about one-third compared to the reference simulation (Figure 4a). This difference cannot solely be explained by a weakening of the wind-driven gyre component calculated from the Sverdrup relation (Figure 4b). Although this relation is not fully accurate near boundaries and topography, our results indicate that the density-driven gyre component is also affected by the large changes in the state of the subpolar North Atlantic.

The largely gyre-related heat and salt transport into the subpolar North Atlantic weakens by about 50% (0.3PW, $0.6 \cdot 10^7$ kg/s) compared to the reference simulation (Figures 5a and 5c). The weakening of the heat and salt transport into the Nordic Seas is of similar magnitude (Figures 5b and 5d) and is mainly caused by a 50% (5 Sv) weaker volume transport of the Atlantic inflow (Figure 7a). Interestingly, the amplitude of the northward salt transport (Figures 5c, 5d, and 7b) is larger under reduced wind stress forcing than in the reference simulation (and under enhanced wind stress forcing). One possible explanation is a larger relative impact of the surface fresh water flux on salinity, as the ocean circulation and associated salt advection are rather weak.

As a consequence of the reduced heat and salt transport, the surface state of the subpolar North Atlantic and Nordic Seas is colder by about 5°C and fresher by 2–3 psu compared to the reference simulation (Figures 12c and 12g). The fresher SSS anomalies in the western subpolar North Atlantic are further supported by the intensified sea ice export from the Nordic Seas through the Denmark Strait, which is three times larger than in the reference simulation (Figure 7c).

In the “0.5windstress” experiment, the winter sea ice extent reaches its maximum extent already in the first decades, and remains unchanged thereafter (Figures 3k and 12k). Accordingly, deep convection in the subpolar and Nordic Seas shuts down already in the first decades and does not recover thereafter (Figures 3m,

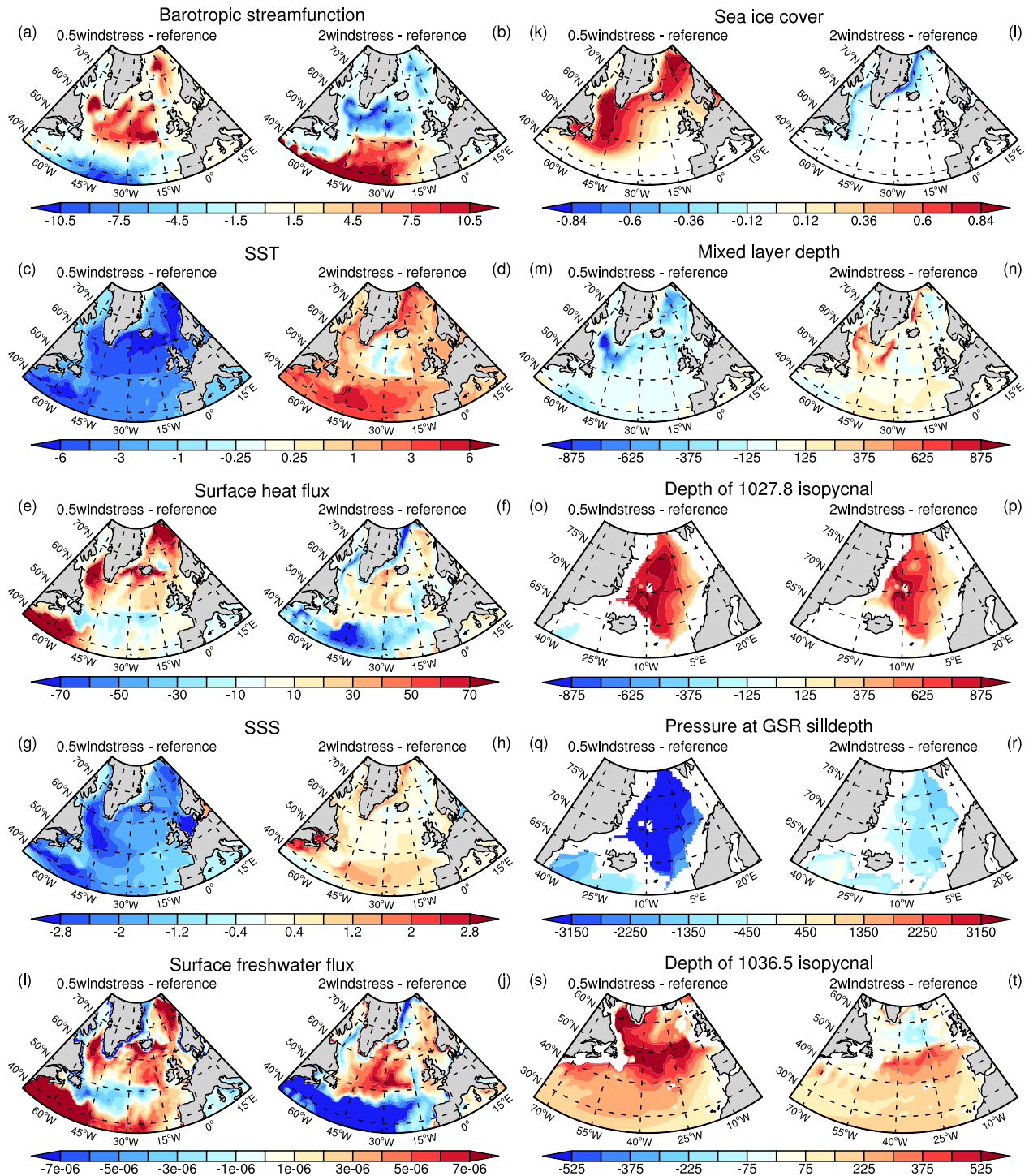


Figure 12. Difference between (left panels) the “0.5windstress” experiment and the reference simulation and (right panels) the “2windstress” experiment and the reference simulation, averaged over integration years 101–250. (a, b) Barotropic streamfunction [in Sv], (c, d) SST [in °C], (e, f) downward surface heat flux [in W/m²], (g, h) SSS [in psu], (i, j) downward surface fresh water flux [in kg/m²s], (k, l) sea ice extent in March [0 to 1, not plotted where sea ice extent is zero in both the respective sensitivity experiment and the reference simulation], (m, n) mixed layer depth in March [in m], (o, p) depth of isopycnal $\sigma_0 = 27.8$ kg/m³ [in m] (upper boundary of overflow water masses), (q, r) baroclinic pressure at 800 m depth [in Pa; defined as hydrostatic pressure integrated over the water column, not taking into account the sea surface height], and (s, t) depth of isopycnal $\sigma_2 = 36.5$ kg/m³ [in m] (center NADW isopycnal). We note that contour levels for SST are nonlinear with values [0.25, 0.5, 1, 2, 3, 4, 5, 6].

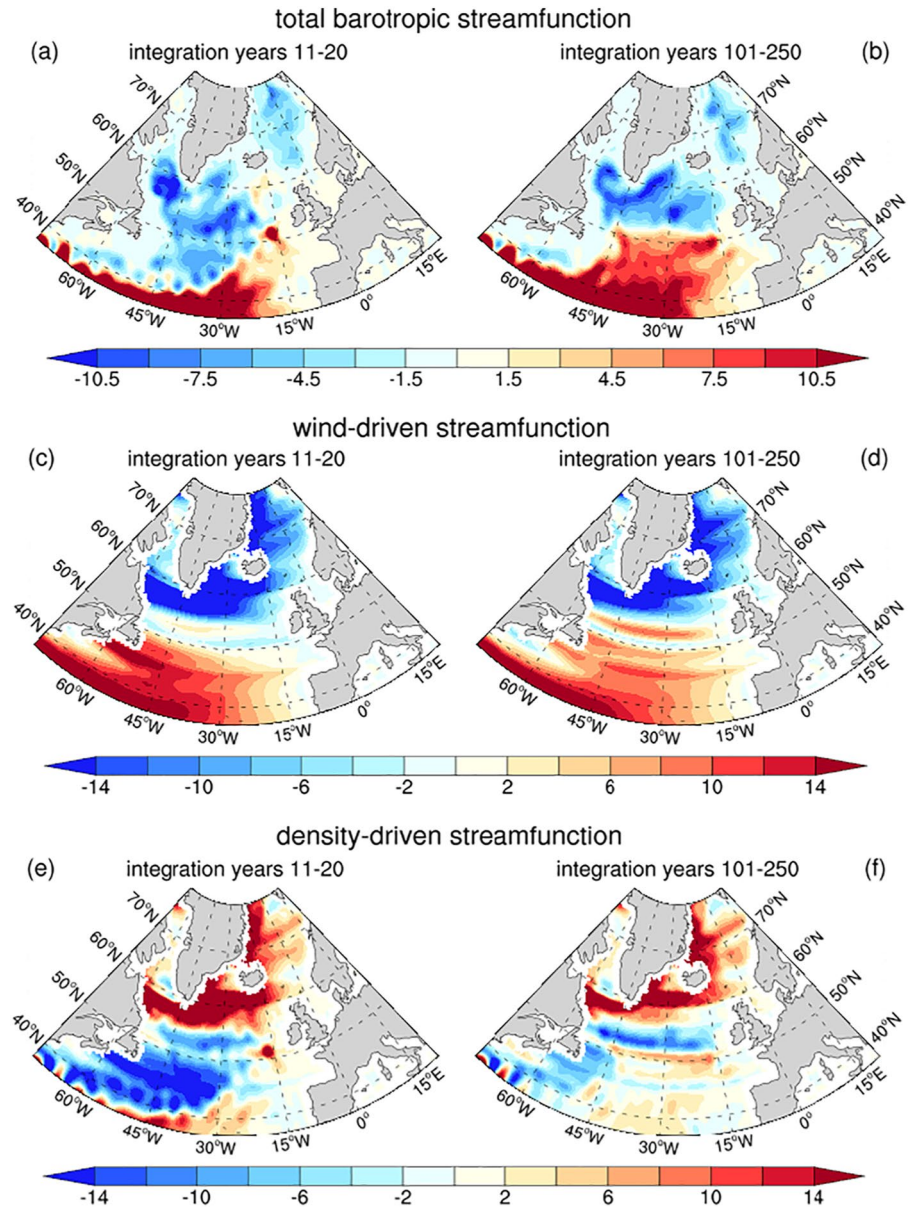


Figure 13. Difference [in Sv] between the “2windstress” experiment and the reference simulation, averaged over integration years (left panels) 11–20 and (right panels) 101–250. (a, b) Barotropic streamfunction, (c, d) wind-driven streamfunction calculated from the Sverdrup relation, and (e, f) density-driven streamfunction defined as the residual between the barotropic and the wind-driven streamfunction. We note that the barotropic streamfunction is identical to Figures 3b and 12b, but is shown here again for easier comparison.

9a,, and 12m). A decrease in subpolar North Atlantic and Nordic Seas surface density by $1\text{--}2\text{ kg m}^{-3}$ (Figure 8a for the western subpolar North Atlantic) further impedes deep convection, as surface density anomalies in the western subpolar North Atlantic are determined by salinity anomalies in the “0.5windstress” experiment (Figure 8c).

A shutdown of deep convection leads to subsurface warming (in contrast to the surface cooling) of the order of 1°C in the temperature averaged over the upper 1,000 m (depth of the maximum AMOC strength) (not shown). Consequently, the isopycnals deepen by approximately 500–1,000 m compared to the reference simulation (Figures 12o and 12s). A strong deepening of the NADW isopycnals by about 1,000 m is consistent with the findings of Cessi (2018) (her Figure 3).

In the Nordic Seas, the deeper stratification results in a decrease in baroclinic pressure at the sill depth of the GSR of up to about 3,500 Pa (Figure 12q), reducing the overflow transports by more than 50% (1–2 Sv) (Figures 11a and 11b). Furthermore, the subsurface ocean warms by about 2–3°C (not shown), which decreases the density of the overflows by about 0.1–0.2 kg m⁻³ (Figures 11c and 11d).

The strong changes in the Nordic Seas overflow and the shutdown of subpolar deep convection result in a much weaker and shallower NADW cell under reduced wind stress forcing compared to the reference simulation (Figures 1a and 1b). As discussed in Putrasahan et al. (2019), the positive salinity advection feedback keeps the AMOC in the weaker state under reduced wind stress forcing: a weaker AMOC further reduces the northward heat and salt transport, enlarging the winter sea ice extent, decreasing the subpolar surface density and reducing the Nordic Seas baroclinic pressure.

5.2. Quasi-Equilibrium Response to Enhanced Wind Stress Forcing

Under enhanced wind stress forcing, the quasi-equilibrium response of the AMOC is similar to the reference simulation (as we discuss in Section 2.2), but the state of the subpolar North Atlantic and Nordic Seas circulation and climate deviates in many aspects.

The subpolar gyre remains stronger in the “2windstress” experiment, largely due to its stronger wind-driven component (Figures 4a and 4b). Interestingly, the heat and salt transport into the subpolar North Atlantic, which in the mean is dominated by the gyre component, is of similar magnitude as in the reference simulation (Figures 5a and 5c). After splitting the transports into MOC component (based on zonal-mean velocity, temperature, and salinity) and gyre component (based on velocity, temperature, and salinity deviations from the zonal-mean), we find that changes in both components approximately compensate each other (not shown).

In contrast, the heat transport into the Nordic Seas is stronger in the “2windstress” experiment compared to the reference simulation (Figure 5b). The resulting heat transport divergence leads to a “warming hole” in the eastern subpolar North Atlantic, not only in SST (Figure 12d), but also in the temperature averaged over the upper 1,000 m (not shown). A subpolar “warming hole” is also described in studies assessing the recent warming trend and future climate in the North Atlantic and linked among others to AMOC changes (Drijfhout et al., 2012; Keil et al., 2020).

Apart from the “warming hole,” the surface state is warmer compared to the reference simulation, and the northern North Atlantic remains largely ice-free in winter in the “2windstress” experiment (Figure 12l). The latter is also supported by a positive feedback, as reduced sea ice extent leads to enhanced wind mixing and a less stable water column, which impedes sea ice formation. As the winter ice-free region expands, so does the area where deep convection occurs in the Labrador Sea (Figure 12n). The maximum convection depth in the Labrador Sea, however, is unchanged compared to the reference simulation (Figure 9b). Deeper convection is found in the Irminger Sea. The influence of variations in Irminger Sea convection on changes in AMOC strength, however, is small in this model setup.

In the subpolar North Atlantic, enhanced surface fresh water input is found compared to the reference simulation (Figure 12j), due to increased precipitation (Figure 6 for the western subpolar North Atlantic; we note that increased evaporation compared to the reference simulation is only found in the western subpolar North Atlantic, likely due to the smaller sea ice extent). The largest increase in subpolar precipitation is found between 50°N and 55°N (not shown) and might be related to a northward shift of the North Atlantic storm track associated with a northward shift of the oceanic gyre boundary (Figure 12b). The surface fresh water input compensates the tendency to increase subpolar salinity due to a salt transport convergence between 50°N and the GSR compared to the reference simulation (Figures 5c and 5d) as well as vanishing sea ice export from the Nordic Seas (Figure 7c).

The enhanced surface fresh water input in the subpolar North Atlantic compared to the reference simulation contributes to the reduced salinity of the Atlantic inflow (Figure 7b) and salt transport across the GSR (Figure 5d). The latter are indeed smaller under enhanced wind stress forcing than in the reference simulation. In addition, there is also a slight surface fresh water input into the eastern part of the Nordic Seas compared to the reference simulation (Figure 12j).

Consequently, fresher conditions for salinity averaged over the upper 1,000 m are found in both the North Atlantic and the Nordic Seas (not shown), leading to a shallowing of the isopycnals (Figures 12p and 12t), except for the subpolar region due to the “warming hole” discussed above. Interestingly, also Cessi (2018) finds a deepening of the zonally averaged center NADW isopycnal south of 40°N, but a shallowing between 40°N and 60°N in the equilibrium response to doubled wind stress forcing over the mid-latitude North Atlantic (her Figure 3), even though the idealized Atlantic basin applied in her study does not resolve the Nordic Seas and the exchanges across the GSR.

In the western subpolar North Atlantic, the lighter subsurface state prevents deep convection to reach deeper than in the reference simulation (Figure 9b). In the Nordic Seas, the deeper stratification leads to a decrease in baroclinic pressure at the sill depth of the GSR compared to the reference simulation (Figure 12r). The reduction in the baroclinic pressure south of the GSR is of similar magnitude, resulting in a pressure gradient across the ridge similar to that in the reference simulation. Thus, the strength of the Nordic Seas overflows is only slightly higher compared to the reference simulation (Figures 11a and 11b) (Hansen & Osterhus, 2007). The fresher subsurface conditions also lead to a small reduction in salinity (not shown) and density (Figures 11c and 11d) of the overflow waters.

Both maximum convection depth in the subpolar North Atlantic and strength and density of the Nordic Seas overflows in the last 150 integration years in the “2windstress” experiment are of comparable magnitude as in the reference simulation, resulting in a similar NADW cell under enhanced wind stress forcing (Figures 1a and 1c). The negative temperature advection feedback prevents the AMOC from strengthening under enhanced wind stress forcing: a stronger AMOC would increase the northward heat transport and decrease the western subpolar surface density and thus weaken deep convection (surface density anomalies in the western subpolar North Atlantic are determined by temperature anomalies after about 50 years in the “2windstress” experiment; Figure 8d).

6. Local Effect of Reduced and Enhanced Wind Stress Forcing on AMOC Strength

In this section, we briefly assess the local effect of reduced and enhanced wind stress forcing on the AMOC strength. We consider the AMOC strength at 26.5°N (Figure 2a) and its decomposition into the wind-driven Ekman component, the Gulf Stream transport, and the density-driven upper mid-ocean transport, as applied to the observed AMOC strength (Kanzow et al., 2007).

The Ekman component is defined as the zonal integral of the meridional Ekman transport ($-\tau_x/f\rho_0$, with τ_x denoting zonal wind stress, f Coriolis parameter and ρ_0 reference density) at 26.5°N in the Atlantic basin. For the Gulf Stream transport, we follow Baehr et al. (2009), and integrate the volume transport over the full width of the boundary current at 26.5°N down to a depth of 1,000 m. We note that this definition differs from Gutjahr et al. (2019), who analyze the same control simulation as in our study and confine the Gulf Stream transport to the section between Florida and the Bahamas, yielding a smaller mean transport. The upper mid-ocean transport is defined as the residual obtained by subtracting the Ekman and Gulf Stream transport from the total AMOC strength at 26.5°N. This simplified method sufficiently approximates the upper mid-ocean transport (Baehr et al., 2009).

As expected from the prescribed wind stress forcing, the strength of the Ekman component in the “0.5windstress” and “2windstress” experiment is about half and twice as strong as in the reference simulation, respectively (Figure 2b). Both Gulf Stream and upper mid-ocean transport also decrease in the “0.5windstress” experiment and increase in the “2windstress” experiment (Figures 2c and 12d; note that the upper mid-ocean transport is southward, i.e., negative). Interestingly, the initial increase of both transports in the “2windstress” experiment is about two times as large as the initial decrease in the “0.5windstress” experiment, which indicates a fast response to the changed wind stress forcing.

In the last 150 integration years in the “0.5windstress” experiment, when the AMOC reaches a quasi-equilibrium response (Figure 2a), the decline in the Gulf Stream transport is larger than that in the (southward directed) upper mid-ocean transport (Figures 2c and 2d). Together with the reduction in the northward Ek-

man component, this transport decline yields a net decrease in the AMOC strength of about 6 Sv (compared to the reference simulation), of which one-third is explained by the changes in the Ekman component.

In contrast, in the “2windstress” experiment, the increase in the Gulf Stream transport is smaller than that in the (southward directed) upper mid-ocean transport. The difference between these two transports compensates the increase in the northward Ekman component, yielding a net AMOC strength similar to the strength in the reference simulation.

7. Discussion and Conclusions

Based on sensitivity experiments with the MPI-ESM1.2 model, we investigate the response of the northern North Atlantic circulation and climate as well as the AMOC to reduced and enhanced wind stress forcing. Under reduced wind stress forcing, the AMOC strength decreases and stabilizes at about half the value found in the reference simulation. In contrast, the AMOC strength under enhanced wind stress forcing increases only initially, then decreases and stabilizes at a value similar to the reference simulation. Thus, our study focuses on three questions:

1. Do the northern North Atlantic circulation and climate as well as the AMOC initially (within a few decades) respond linearly to reduced and enhanced wind stress forcing?

Under reduced wind stress forcing, a spin-down of the North Atlantic gyre circulation leads to decreased northward heat and salt transport, and thus to larger winter sea ice extent and a shutdown of subpolar deep convection. In the Nordic Seas, the fresher and lighter subsurface state leads to a decrease in the baroclinic pressure and a weakening of the overflows across the GSR. Under enhanced wind stress forcing, initially the opposite is happening. Thus, the initial response of the northern North Atlantic circulation and climate as well as the AMOC to reduced and enhanced wind stress forcing is approximately linear.

2. Why is the AMOC strength decreasing (after the initial increase) under enhanced wind stress forcing?

Under enhanced wind stress forcing, surface density anomalies in the western subpolar North Atlantic are eventually determined by temperature rather than salinity anomalies, which leads to a decrease in surface density and to a weakening of subpolar deep convection. In the Nordic Seas, the saltier and denser subsurface state is gradually replaced by a fresher and lighter state, resulting in a decrease in the baroclinic pressure and a weakening of the overflows across the GSR. The gradual freshening is caused by a decrease in the salinity of the Atlantic inflow, probably related to the AMOC weakening triggered by subpolar deep convection changes.

3. What is the quasi-equilibrium response of the northern North Atlantic circulation and climate as well as the AMOC under reduced and enhanced wind stress forcing? To what extent differs the quasi-equilibrium response of the northern North Atlantic circulation and climate under enhanced wind stress forcing from the reference simulation, even though the AMOC strength converges?

In contrast to the initial response, the quasi-equilibrium response of the subpolar North Atlantic and Nordic Seas circulation and climate to reduced and enhanced wind stress forcing is nonlinear. Under reduced wind stress forcing, the quasi-equilibrium response is similar to the initial response, with even larger changes compared to the reference simulation. In addition, a strong subsurface warming is found due to reduced winter heat loss to the atmosphere and shutdown of deep convection, which strongly reduces the density of the Nordic Seas overflows.

Under enhanced wind stress forcing, the northern North Atlantic exhibits a warmer (sub)surface state compared to the reference simulation, except for a “warming hole” in the eastern subpolar North Atlantic. In the area of the “warming hole” as well as in the eastern Nordic Seas, surface fresh water input is found compared to the reference simulation, leading to a fresher and (except in the area of the “warming hole”) lighter subsurface state. Although deep convection area increases in the subpolar North Atlantic due to smaller winter sea ice extent, the maximum convection depth is similar to the reference simulation. In the Nordic Seas, the lighter subsurface state leads to a decrease in the baroclinic pressure. However, the decrease south of the GSR is of similar magnitude, resulting in a Nordic Seas overflow transport, which is only slightly higher compared to the reference simulation.

Key to the response of the northern North Atlantic circulation and climate described in our study is the changed wind stress forcing over the North Atlantic. Thus our results indicate possible impacts of a future intensification or weakening of the northern hemispheric jet stream and associated North Atlantic storm track on the large-scale North Atlantic circulation and climate.

Since our study is model-based, there are possible caveats that are shortly discussed in the following. The response of the AMOC in the wind sensitivity experiments is largely driven by changes in deep convection in the Labrador Sea. Like most state-of-the-art climate models (Heuze, 2017, 2021), our model simulates slightly too deep and too far south reaching convection in the Labrador Sea (Gutjahr et al., 2019). Also, the representation of the overflows from the Nordic Seas, which contribute to the AMOC response in the wind sensitivity experiments, is generally biased in state-of-the-art climate models (Heuze, 2021; Yeager & Danabasoglu, 2012).

Furthermore, the AMOC strength in the “2windstress” experiment depends largely on how the surface density anomalies in the western subpolar North Atlantic are determined. Surface density anomalies are initially controlled by salinity anomalies, but after a couple of decades temperature anomalies dominate. However, models do not agree on what determines the surface density anomalies in the subpolar North Atlantic—alinity (Danabasoglu et al., 2012; Delworth et al., 1993; Dong & Sutton, 2005; Jungclaus et al., 2005), temperature (Bentsen et al., 2004; Zhu & Jungclaus, 2008), or both (Danabasoglu, 2008).

Most importantly, there is recent evidence that the influence of Labrador Sea deep convection on AMOC variability is overestimated in state-of-the-art climate models (Chafik & Rossby, 2019; Li et al., 2019; Lozier et al., 2019; Menary et al., 2020; Zou et al., 2020). There is also emerging evidence that resolving ocean mesoscale eddies is crucial for a realistic simulation of the export of convective water masses (Brueggemann & Katsman, 2019; Georgiou et al., 2019) and also influences the mean state and variability of the AMOC (Hewitt et al., 2020; Johnson et al., 2019).

For more robust results, especially regarding the response to enhanced wind stress forcing, the presented analysis should thus be repeated with other climate models. More insights are especially expected from including ocean eddy-resolving grid configurations.

Data Availability Statement

The MPI-ESM1.2 simulations used in this study are available from the CERA-LTA-DOKU databank at the German Climate Computing Center (DKRZ) via the links given below. Registration is required to download the data. “0.5windstress”: cera-www.dkrz.de/WDCC/ui/Compact.jsp?acronym=DKRZ_LTA_944_ds00015. “2windstress”: cera-www.dkrz.de/WDCC/ui/Compact.jsp?acronym=DKRZ_LTA_944_ds00016. reference: cera-www.dkrz.de/WDCC/ui/Compact.jsp?acronym=DKRZ_LTA_944_ds00011. <https://www.agu.org/Publish-with-AGU/Publish/Author-Resources/Data-and-Software-for-AuthorsIGSN>.

References

- Adcroft, A., Hill, C., & Marshall, J. (1997). Representation of topography by shaved cells in a height coordinate ocean model. *Monthly Weather Review*, 125, 2293–2315. [https://doi.org/10.1175/1520-0493\(1997\)125<2293:rotbsc>2.0.co;2](https://doi.org/10.1175/1520-0493(1997)125<2293:rotbsc>2.0.co;2)
- Ba, J., Keenlyside, N., Park, W., Latif, M., Hawkins, E., & Ding, H. (2013). A mechanism for atlantic multidecadal variability in the Kiel Climate Model. *Climate Dynamics*, 41, 2133–2144. <https://doi.org/10.1007/s00382-012-1633-4>
- Baehr, J., Cunningham, S., Haak, H., Heimbach, P., Kanzow, T., & Marotzke, J. (2009). Observed and simulated estimates of the meridional overturning circulation at 26.5n in the Atlantic. *Ocean Science*, 5, 575–589. <https://doi.org/10.5194/os-5-575-2009>
- Bentsen, M., Drange, H., Furevik, T., & Zhou, T. (2004). Simulated variability of the Atlantic meridional overturning circulation. *Climate Dynamics*, 22, 701–720. <https://doi.org/10.1007/s00382-004-0397-x>
- Bjostoch, A., Boening, C., Getzlaff, J., Molines, J., & Madec, G. (2008). Causes of interannual-decadal variability in the meridional overturning circulation of the midlatitude North Atlantic Ocean. *Journal of Climate*, 21, 6599–6615. <https://doi.org/10.1175/2008JCLI2404.1>
- Bjostoch, A., Kaese, R., & Stammer, D. (2003). The sensitivity of the Greenland–Scotland ridge overflow to forcing changes. *Journal of Physical Oceanography*, 33, 2307–2319. [https://doi.org/10.1175/1520-0485\(2003\)033<2307:tsotgr>2.0.co;2](https://doi.org/10.1175/1520-0485(2003)033<2307:tsotgr>2.0.co;2)
- Broecker, W. (1998). Paleoocean circulation during the last deglaciation: A bipolar seesaw? *Paleoceanography*, 13, 119–121. <https://doi.org/10.1029/97PA03707>
- Brueggemann, N., & Katsman, C. (2019). Dynamics of downwelling in an eddying marginal sea: Contrasting the Eulerian and the isopycnal perspective. *Journal of Physical Oceanography*, 49, 3017–3035. <https://doi.org/10.1175/JPO-D-19-0090.1>
- Buckley, M., & Marshall, J. (2016). Observations, inferences, and mechanisms of the Atlantic meridional overturning circulation: A review. *Reviews of Geophysics*, 54, 5–63. <https://doi.org/10.1002/2015RG000493>

Acknowledgments

The research leading to these results has received funding from the European Union by the H2020 Framework Program under grant agreements no. 641727 (PRIMAVERA project) as well as from the German Federal Ministry of Education and Research (BMBF) through JPI Climate/JPI Oceans NextG-Climate Science-ROADMAP (FKZ: 01LP2002A) and BMBF program “RACE” (FKZ: 03F0824D). The authors wish to thank Xiuhua Zhu and Veit Lueschow for valuable comments on an earlier version of the manuscript. The simulations were conducted at DKRZ. Open access funding enabled and organized by Projekt DEAL.

- Cessi, P. (2018). The effect of northern hemisphere winds on the meridional overturning circulation and stratification. *Journal of Physical Oceanography*, 48, 2495–2506. <https://doi.org/10.1175/JPO-D-18-0085.1>
- Chafik, L., & Rossby, T. (2019). Volume, heat, and freshwater divergences in the subpolar North Atlantic suggest the nordic seas as key to the state of the meridional overturning circulation. *Geophysical Research Letters*, 46, 4799–4808. <https://doi.org/10.1029/2019GL082110>
- Danabasoglu, G. (2008). On multidecadal variability of the Atlantic meridional overturning circulation in the community climate system model version 3. *Journal of Climate*, 21, 5524–5544. <https://doi.org/10.1175/2008JCLI2019.1>
- Danabasoglu, G., Yeager, S., Kwon, Y., Tribbia, J., Phillips, A., & Hurrell, J. (2012). Variability of the Atlantic meridional overturning circulation in CCSM4. *Journal of Climate*, 25, 5153–5172. <https://doi.org/10.1175/JCLI-D-11-00463.1>
- Delworth, T., Manabe, S., & Stouffer, R. (1993). Interdecadal variations of the thermohaline circulation in a coupled ocean-atmosphere model. *Journal of Climate*, 6, 1993–2011. [https://doi.org/10.1175/1520-0442\(1993\)006<1993:ivottc>2.0.co;2](https://doi.org/10.1175/1520-0442(1993)006<1993:ivottc>2.0.co;2)
- Delworth, T., & Zeng, F. (2008). Simulated impact of altered southern hemisphere winds on the Atlantic meridional overturning circulation. *Geophysical Research Letters*, 35, L20708. <https://doi.org/10.1029/2008GL035166>
- Dickson, R., & Brown, J. (1994). The production of North Atlantic deep water: Sources, rates, and pathways. *Journal of Geophysical Research*, 99, 12319–12341. <https://doi.org/10.1029/94JC00530>
- Dong, B., & Sutton, R. (2005). Mechanism of interdecadal thermohaline circulation variability in a coupled ocean-atmosphere GCM. *Journal of Climate*, 18, 1117–1135. <https://doi.org/10.1175/JCLI3328.1>
- Drijfhout, S., van Oldenborgh, G., & Cimadoribus, A. (2012). Is a decline of AMOC causing the warming hole above the North Atlantic in observed and modeled warming patterns? *Journal of Climate*, 25, 8373–8379. <https://doi.org/10.1175/JCLI-D-12-00490.1>
- Eden, C., & Willebrand, J. (2001). Mechanism of interannual to decadal variability of the North Atlantic circulation. *Journal of Climate*, 14, 2266–2280. [https://doi.org/10.1175/1520-0442\(2001\)014<2266:moitdv>2.0.co;2](https://doi.org/10.1175/1520-0442(2001)014<2266:moitdv>2.0.co;2)
- Evans, D., Toole, J., Forget, G., Zika, J., Garabato, A., Nurser, A., & Yu, L. (2017). Recent wind-driven variability in Atlantic water mass distribution and meridional overturning circulation. *Journal of Physical Oceanography*, 47, 633–647. <https://doi.org/10.1175/JPO-D-16-0089.1>
- Eyring, V., Bony, S., Meehl, G., Senior, C., Stevens, B., Stouffer, R., & Taylor, K. (2016). Overview of the coupled model intercomparison project phase 6 (CMIP6) experimental design and organization. *Geoscientific Model Development*, 9, 1937–1958. <https://doi.org/10.5194/gmd-9-1937-2016>
- Frankignoul, C., Deshayes, J., & Curry, R. (2009). The role of salinity in the decadal variability of the North Atlantic meridional overturning circulation. *Climate Dynamics*, 33, 777–793. <https://doi.org/10.1007/s00382-008-0523-2>
- Georgiou, S., van der Boog, C., Brueggemann, N., Ypma, S., Pietrzak, J., & Katsman, C. (2019). On the interplay between downwelling, deep convection and mesoscale eddies in the Labrador Sea. *Ocean Modelling*, 135, 56–70. <https://doi.org/10.1016/j.ocemod.2019.02.004>
- Good, S., Martin, M., & Rayner, N. (2013). En4: Quality controlled ocean temperature and salinity profiles and monthly objective analyses with uncertainty estimates. *Journal of Geophysical Research: Oceans*, 118, 6704–6716. <https://doi.org/10.1002/2013JC009067>
- Gutjahr, O., Brueggemann, N., Haak, H., Jungclauss, J., Putrasahan, D., Lohmann, K., & von Storch, J. (2021). Comparison of ocean vertical mixing schemes in the Max Planck Institute Earth System Model (MPI-ESM1.2). *Geoscientific Model Development*, 14, 2317–2349. <https://doi.org/10.5194/gmd-14-2317-2021>
- Gutjahr, O., Putrasahan, D., Lohmann, K., Jungclauss, J., von Storch, J., Brueggemann, N., et al. (2019). Max Planck Institute Earth System Model (MPI-ESM1.2) for the High-Resolution model intercomparison project (HighResMIP). *Geoscientific Model Development*, 12, 3241–3281. <https://doi.org/10.5194/gmd-12-3241-2019>
- Haarsma, R., Roberts, M., Vidale, P., Senior, C., Bellucci, A., Bao, Q., et al. (2016). High resolution model intercomparison project (HighResMIP v1.0) for cmip6. *Geoscientific Model Development*, 9, 4185–4208. <https://doi.org/10.5194/gmd-9-4185-2016>
- Hansen, B., & Osterhus, S. (2007). Faroe bank channel overflow 1995–2005. *Progress in Oceanography*, 75, 817–856. <https://doi.org/10.1016/j.pocean.2007.09.004>
- Heuze, C. (2017). North Atlantic deep water formation and AMOC in cmip5 models. *Ocean Science*, 13, 609–622. <https://doi.org/10.5194/os-13-609-2017>
- Heuze, C. (2021). Antarctic bottom water and North Atlantic deep water in cmip6 models. *Ocean Science*, 17, 59–90. <https://doi.org/10.5194/os-17-59-2021>
- Hewitt, H., Roberts, M., Mathiot, P., Biastoch, A., Blockley, E., Chassignet, E., et al. (2020). Resolving and parameterising the ocean mesoscale in Earth system models. *Current Climate Change Reports*, 6, 137–152. <https://doi.org/10.1007/s40641-020-00164-w>
- Jackson, L., & Vellinga, M. (2012). Multidecadal to centennial variability of the AMOC: HadCM3 and a perturbed physics ensemble. *Journal of Climate*, 26, 2390–2407. <https://doi.org/10.1175/JCLI-D-11-00601.1>
- Johnson, H., Cessi, P., Marshall, D., Schloesser, F., & Spall, M. (2019). Recent contributions of theory to our understanding of the Atlantic meridional overturning circulation. *Journal of Geophysical Research: Oceans*, 124, 5376–5399. <https://doi.org/10.1029/2019JC015330>
- Jungclauss, J., Haak, H., Latif, M., & Mikolajewicz, U. (2005). Arctic–North Atlantic interactions and multidecadal variability of the meridional overturning circulation. *Journal of Climate*, 18, 4013–4031. <https://doi.org/10.1175/JCLI3462.1>
- Jungclauss, J., Macrander, A., & Kaese, R. (2008). *Arctic–subarctic ocean fluxes: Defining the role of the Northern Seas in climate* (p. 527–549). Springer Verlag.
- Kanzow, T., Cunningham, S., Rayner, D., Hirschi, J., Johns, W., Baringer, M., et al. (2007). Observed flow compensation associated with the moc at 26.5n in the Atlantic. *Science*, 317, 938–941. <https://doi.org/10.1126/science.1141304>
- Keil, P., Mauritsen, T., Jungclauss, J., Hedemann, C., Olonscheck, D., & Ghosh, R. (2020). Multiple drivers of the North Atlantic warming hole. *Nature Climate Change*, 10, 667–671. <https://doi.org/10.1038/s41558-020-0819-8>
- Klinger, B., Drijfhout, S., Marotzke, J., & Scott, J. (2003). Sensitivity of basinwide meridional overturning to diapycnal diffusion and remote wind forcing in an idealized Atlantic–Southern Ocean geometry. *Journal of Physical Oceanography*, 33, 249–266. [https://doi.org/10.1175/1520-0485\(2003\)033<0249:sobmot>2.0.co;2](https://doi.org/10.1175/1520-0485(2003)033<0249:sobmot>2.0.co;2)
- Koehl, A. (2005). Anomalies of meridional overturning: Mechanisms in the North Atlantic. *Journal of Physical Oceanography*, 35, 1455–1472. <https://doi.org/10.1175/JPO2767.1>
- Koehl, A., & Stammer, D. (2008). Variability of the meridional overturning in the North Atlantic from the 50-year GECCO state estimation. *Journal of Physical Oceanography*, 38, 1913–1930. <https://doi.org/10.1175/2008JPO3775.1>
- Li, F., Lozier, M., Danabasoglu, G., Holliday, N., Kwon, Y., Romanou, A., et al. (2019). Local and downstream relationships between Labrador sea water volume and North Atlantic meridional overturning circulation variability. *Journal of Climate*, 32, 3883–3898. <https://doi.org/10.1175/JCLI-D-18-0735.1>
- Lozier, M., Li, F., Bacon, S., Bahr, F., Bower, A., Cunningham, S., et al. (2019). A sea change in our view of overturning in the subpolar North Atlantic. *Science*, 363, 516–521. <https://doi.org/10.1126/science.aau6592>

- Lueschow, V., Marotzke, J., & von Storch, J. (2021). Overturning response to a surface wind stress doubling in an eddying and a non-eddying ocean. *Journal of Physical Oceanography*, *51*, 1007–1020. <https://doi.org/10.1175/JPO-D-20-0176.1>
- Marshall, J., Scott, J., Romanou, A., Kelley, M., & Leboissetier, A. (2017). The dependence of the ocean's moc on mesoscale eddy diffusivities: A model study. *Ocean Modelling*, *111*, 1–8. <https://doi.org/10.1016/j.ocemod.2017.01.001>
- Marshall, J., & Speer, K. (2012). Closure of the meridional overturning circulation through southern ocean upwelling. *Nature Geoscience*, *5*, 171–180. <https://doi.org/10.1038/ngeo1391>
- Mauritsen, T., Bader, J., Becker, T., Behrens, J., Bittner, M., Brokopf, R., et al. (2019). Developments in the MPI-M Earth System Model version 1.2 (MPI-ESM1.2) and its response to increasing CO₂. *Journal of Advances in Modeling Earth Systems*, *11*, 998–1038. <https://doi.org/10.1029/2018MS001400>
- Mauritzen, C., & Haekkinen, S. (1999). On the relationship between dense water formation and the “meridional overturning cell” in the North Atlantic Ocean. *Deep-Sea Research Part I*, *46*, 877–894. [https://doi.org/10.1016/S0967-0637\(98\)00094-6](https://doi.org/10.1016/S0967-0637(98)00094-6)
- Medhaug, I., Langehaug, H., Eldevik, T., Furevik, T., & Bentsen, M. (2012). Mechanisms for decadal scale variability in a simulated Atlantic meridional overturning circulation. *Climate Dynamics*, *39*, 77–93. <https://doi.org/10.1007/s00382-011-1124-z>
- Menary, M., Jackson, L., & Lozier, M. (2020). Reconciling the relationship between the AMOC and Labrador Sea in OSNAP observations and climate models. *Geophysical Research Letters*, *47*, e2020GL089793. <https://doi.org/10.1029/2020GL089793>
- Mikolajewicz, U., & Voss, R. (2000). The role of the individual air-sea flux components in CO₂-induced changes of the ocean's circulation and climate. *Climate Dynamics*, *16*, 627–642. <https://doi.org/10.1007/s003820000066>
- Msadek, R., & Frankignoul, C. (2009). Atlantic multidecadal oceanic variability and its influence on the atmosphere in a climate model. *Climate Dynamics*, *33*, 45–62. <https://doi.org/10.1007/s00382-008-0452-0>
- Mueller, W., Jungclaus, J., Mauritsen, T., Baehr, J., Bittner, M., Budich, R., et al. (2018). A higher-resolution version of the Max Planck Institute Earth System Model (MPI-ESM1.2-hr). *Journal of Advances in Modeling Earth Systems*, *10*, 1383–1413. <https://doi.org/10.1029/2017MS001217>
- Putrasahan, D., Lohmann, K., von Storch, J., Jungclaus, J., Gutjahr, O., & Haak, H. (2019). Surface flux drivers for the slowdown of the Atlantic meridional overturning circulation in a high-resolution global coupled climate model. *Journal of Advances in Modeling Earth Systems*, *11*, 1349–1363. <https://doi.org/10.1029/2018MS001447>
- Rohrschneider, T., Baehr, J., Lueschow, V., Putrasahan, D., & Marotzke, J. (2021). The depth scales of the AMOC on a decadal timescale. *Ocean Science*. <https://doi.org/10.5194/os-2020-124>
- Toggweiler, J., & Samuels, B. (1995). Effect of drake passage on the global thermohaline circulation. *Deep-Sea Research Part I*, *42*, 477–500. [https://doi.org/10.1016/0967-0637\(95\)00012-U](https://doi.org/10.1016/0967-0637(95)00012-U)
- Wolff, J., Maier-Reimer, E., & Legutke, S. (1997). The Hamburg ocean primitive equation model hope. *Technical Report German Climate Computer Center (DKRZ)*, *13*, 1–97. <https://doi.org/10.2312/WDCC/DKRZn>
- Xu, X., Chassignet, E., Johns, W., Schmitz, W., & Metzger, E. (2014). Intraseasonal to interannual variability of the Atlantic meridional overturning circulation from eddy-resolving simulations and observations. *Journal of Geophysical Research: Oceans*, *119*, 5140–5159. <https://doi.org/10.1002/2014JC009994>
- Yeager, S., & Danabasoglu, G. (2012). Sensitivity of Atlantic meridional overturning circulation variability to parameterized Nordic sea overflows in ccsm4. *Journal of Climate*, *25*, 2077–2103. <https://doi.org/10.1175/JCLI-D-11-00149.1>
- Zhang, R., Delworth, T., Rosati, A., Anderson, W., Dixon, K., Lee, H., & Zeng, F. (2011). Sensitivity of the North Atlantic Ocean circulation to an abrupt change in the nordic sea overflow in a high resolution global coupled climate model. *Journal of Geophysical Research*, *116*, C12024. <https://doi.org/10.1029/2011JC007240>
- Zhu, X., & Jungclaus, J. (2008). Interdecadal variability of the meridional overturning circulation as an ocean internal mode. *Climate Dynamics*, *31*, 731–741. <https://doi.org/10.1007/s00382-008-0383-9>
- Zou, S., Lozier, M., Li, F., Abernathey, R., & Jackson, L. (2020). Density-compensated overturning in the Labrador Sea. *Nature Geoscience*, *13*, 121–126. <https://doi.org/10.1038/s41561-019-0517-1>